Thesis for the Degree of Master of Physics

Synthesis and luminescence characterization of rare earth ions (Tb^{3+}, Sm^{3+}) doped in $Sr_9La_{1-x}(PO_4)_7$ phosphors

by

Eunhye Yang

Department of Physics

The Graduate School

Pukyong National University

February 2020

Synthesis and luminescence characterization of rare earth ions (Tb^{3+}, Sm^{3+}) doped in $Sr_9La_{1-x}(PO_4)_7$ phosphors
(희토류 이온(Tb^{3+}, Sm^{3+})이 첨가된 $Sr_9La_{1-x}(PO_4)_7$ 형광체의 합성과 형광특성 연구)

Advisor: Prof. Sung Heum Park

by
Eunhye Yang

A thesis submitted in partial fulfillment of the requirements
for the degree of

Master of Physics

in Department of Physics, The Graduate School,
Pukyong National University

February 2020

Synthesis and luminescence characterization of rare earth ions (Tb^{3+}, Sm^{3+}) doped in $Sr_9La_{1-x}(PO_4)_7$ phosphors

A dissertation

by

Eunhye Yang

Approved by:

_____

(Chairman) Jung Hyun Jeong

_____ _____

(Member) Jung Hwan Kim (Member) Sung Heum Park

February 22, 2020

Contents

Table Contents

Figure Contents

Synthesis and luminescence characterization of rare earth ions (Tb^{3+}, Sm^{3+}) doped in $Sr_9La_{1-x}(PO_4)_7$ phosphors

Eunhye Yang

Department of Physics, The Graduate School

Pukyong National University

Abstract

The $Sr_9La(PO_4)_7$ phosphors with different doping concentrations of Tb^{3+} and Sm^{3+} were prepared by a solid-state reaction method, respectively. The correlation between crystal structure and photoluminescence (PL) properties of the phosphors were investigated in detail.

Sm^{3+}-doped in $Sr_9La(PO_4)_7$ phosphors was crystallized in a rhombohedral structure. Under the excitation wavelength of 399 nm, $Sr_9La(PO_4)_7$: xSm^{3+} exhibited an intense orange-red emission spectrum centered at 556 nm, 595nm, and 670 nm, which can be assigned to radiation transitions from $^4G_{5/2}$ to $^6H_{5/2}$, $^6H_{7/2}$ and $^6H_{9/2}$ of Sm^{3+}, respectively. The optimal Sm^{3+} doping content was found to be 3 mol%. The concentration quenching mechanism between Sm^{3+} ions was attributed to the dipole-dipole interaction and the critical distance of Sm^{3+} was determined to be 21.917Å. The results indicate that $Sr_9La(PO_4)_7$: xSm^{3+}

phosphors could be promising candidates as orange-red phosphors for being integrated into white light-emitting diodes.

The samples of $Sr_9La(PO_4)_7$: xTb^{3+} were synthesized by a solid-state reaction method. From the XRD pattern analysis, it was confirmed that the crystal structure of samples changed from the rhombohedral (space group $R\bar{3}m$) to the monoclinic (space group I2/a) with an increase of the x value. To obtain crystal structure information, the Rietveld refinement and high-resolution transmission electron microscope (HRTEM) of $Sr_9La(PO_4)_7$: xTb^{3+} (x= 0, 1) were performed. It was found that $Sr_9La_{1-x}(PO_4)_7$: xTb^{3+} phosphors have a broad excitation band at the 200–300 nm region due to the $4f^8 \rightarrow 4f^7 5d^1$ transitions of Tb^{3+} ions. Under the excitation of 376 nm, Tb^{3+}-doped $Sr_9La(PO_4)_7$ shows green emission with a main peak at 542 nm. As increasing of concentration of Tb^{3+} ions up to 100 mol%, the PL intensity of Tb^{3+}-doped in $Sr_9La(PO_4)_7$ was increased, moreover, the decay time of the $Sr_9La(PO_4)_7$: Tb^{3+} phosphor abnormally increased from 2204 μs to 4062 μs. The results indicate that $Sr_9La(PO_4)_7$: Tb^{3+} could be an excellent candidate as a green-emitting phosphor.

1. Introduction

Phosphor-converted light-emitting diodes (pc-LEDs) have attracted great attention in lighting and display fields [1–3]. Due to their advantages, such as high luminescence efficiency, low energy consumption, high physical and chemical stability, and environmental friendliness, the light source based on white LEDs has broad potential applications [4–7].

Currently, there are mainly two methods to achieve white light through the phosphor-converted white LED. The first method is by combining a lnGaN-based blue LED chip with a yellow-emitting $Y_3Al_5O_{12}$: Ce^{3+} (YAG: Ce) phosphor. The advantages of this method are its simple process and inexpensive. However, this combination is disadvantageous in that the color-rendering index is low, and the red light is weak [8–11]. The second method to solve the above problem is to cover the surface of the ultraviolet (UV) chip with three kinds of red, blue, and green phosphors to obtain a white color. Compared to the previous method, the latter method has improved the color-rendering index for full-spectrum lighting. It is essential to find new phosphors with red, green, and blue emission under near-UV excitation.

To obtain a phosphor with high intensity, quenching at a relatively high doping concentration is needed. This concentration quenching strongly depends on the crystal structure environment [12]. Therefore, the choice of the host plays a key role in phosphor efficiency. Recently, several examples of phosphates having a whitlockite crystal structure based on the $M_9R(PO_4)_7$ compound (M= Ca or Sr

and R= La, y, Sc, Gd, or Bi) are applicable as host materials [13]. Specifically, such phosphate compounds have good thermal stability and have complete charge stabilization permitted by the rigid tetrahedral matrix of phosphate [14, 15]. This structure can weaken the possibility of concentration quenching.

Generally, trivalent rare earth ions can emit various colors. Among these, Eu^{3+} and Sm^{3+} have been known as a red activator in phosphors due to the 4f-4f transitions [16, 17]. However, phosphors doped with Eu^{3+} exhibits efficient luminescence only at n-UV excitation, thus limiting application to w-LED. While phosphors doped with Sm^{3+} can be more easily excited from UV to blue region radiation and intense emission intensity in the orange-red region but also present a high color purity of the emitting light because of their sharp characteristic emission spectrum when excited by n-UV radiation [18, 19]. Therefore, the Sm^{3+} doped compounds can be widely applied in temperature sensors, photoluminescence glasses devices, radiation dosimeters, w-LEDs, and so on.

Among the above-mentioned tricolor phosphors, trivalent terbium (Tb^{3+}) is known as an activator of green luminescent materials due to its ^7F_J, $^5D_3$, and $^5D_4$ states. The Tb^{3+} ion has a $4f^8$ electronic configuration in the ground state and a $4f^7$, $5d^1$ electronic configuration in the excited state. Excitation occurs after the absorption of energy, and electronic transitions take place from $4f^8$ to $4f^75d^1$. When the terbium ion returns to its ^7F_J ground level from $^5D_4$, the lowest excited level, it gives rise to characteristic f–f emission transitions. The green emission of Tb^{3+} is the result of the $^5D_4 \rightarrow {}^7F_J$ transition, and the blue emission corresponds to the $^5D_3 \rightarrow {}^7F_J$ transition [20].

In this work, the $Sr_9La(PO_4)_7$: RE^{3+} (RE= Tb^{3+}, Sm^{3+}) phosphors are prepared by using a solid-state method. The prepared samples were characterized by using X-ray diffraction (XRD). The crystal structure information was analyzed based on the Rietveld refinement results. As function of the concentration of Tb^{3+} and Sm^{3+} ions, the photoluminescence (PL) properties of the phosphors related to the crystal structure transformation were studied.

. Theoretical background

2.1 Luminescence mechanisms

A luminescent material, also called a phosphor, is a solid which converts certain types of energy into electromagnetic radiation over and above thermal radiation. When you heat a solid to a temperature over about 600 , it emits red radiation. This is thermal radiation. The electromagnetic radiation emitted by a luminescent material is usually in the visible range, but can also be in other spectral regions, such as the ultraviolet or infrared. Luminescence can be excited by many types of energy. Photoluminescence is excited by electromagnetic radiation, cathodoluminescence by a beam of energetic electrons, electroluminescence by an electric voltage, triboluminescence by mechanical energy, X-ray luminescence by X rays, chemiluminescence by the energy of a chemical reaction, and so on.

The process in the luminescent materials is shown in Fig. 2.1. The luminescent consists of a host lattice and a luminescent center often called an activator. The luminescence processes are as follows. The exciting radiation is absorbed by the activator, raising it to an excited state (Fig. 2.2). The excited state returns to the ground state by emission of radiation. This suggests that every ion and every material shows luminescence. This is not the case. The reason for this is that the radiative emission process has a competitor, viz. the non-radiative return to the ground state. In that process, the energy of the excited state is used to excite the

vibrations of the host lattice, i.e., to heat the host lattice. To create efficient luminescent materials, it is necessary to suppress this non-radiative process.

Sometimes, the exciting radiation is not absorbed by the activator, but elsewhere. We can add another ion to the host lattice. This ion may absorb the exciting radiation and subsequently transfer it to the activator. In this case, the absorbing ion is called a sensitizer. Fig. 2.3 shows the luminescence processes in such a system. The $S \rightarrow S^*$ transition is the absorption (or excitation), the $A_2^* \rightarrow A$ transition the emission. Energy transfer (ET) from level S^* to the level A_1^*, subsequently, the A_1^* level decays non-radiatively to the slightly lower A_2^* level. This process prevents back transfer.

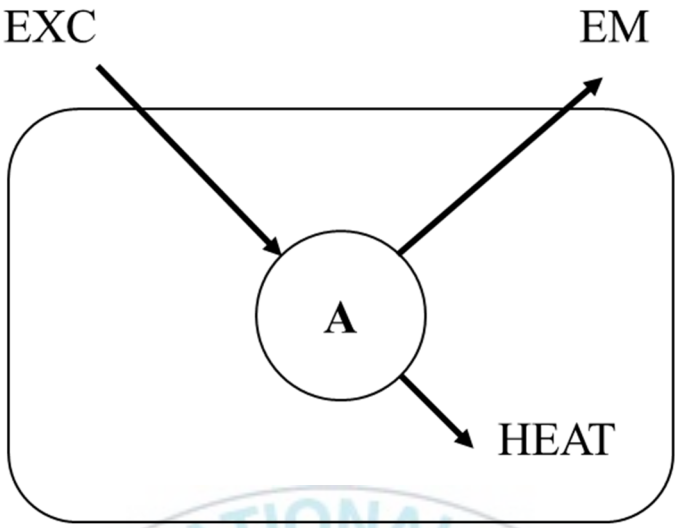

Fig. 2.1 A luminescent ion A in its host lattice. EXC: excitation; EM: emission (radiative return to the ground state); HEAT: non-radiative return to the ground state.

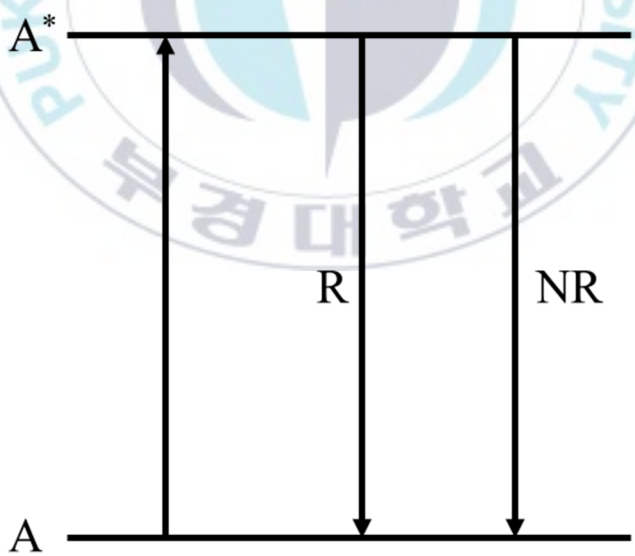

Fig. 2.2 Schematic energy level scheme of the luminescent ion A in Fig. 2.1. The asterisk indicates the excited state, R the radiative return, and NR the non-radiative return to the ground state.

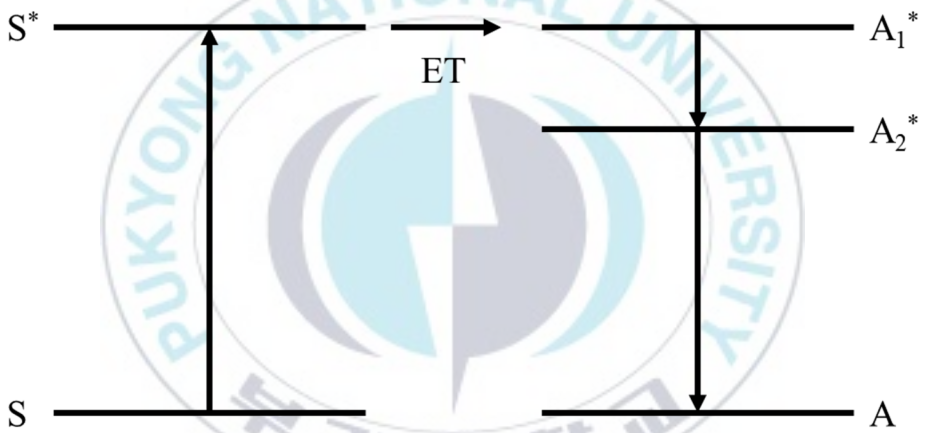

Fig. 2.3 Energy transfer from S (sensitizer) to A (activator).

2.2 Luminescence of rare earth ions

2.2.1 Electronic configurations

Rare earth ions referred to as the lanthanides, comprise the series of elements in the sixth row of the periodic table stretching from Lanthanum (Z=57) to Lutetium (Z=71). These are characterized by [Xe] $4f^{1-14}$, $5s^2$, $5p^6$, and $6s^2$ electronic configuration: all of them have the same outer shell configuration, namely $5s^2$, $5p^6$, and $6s^2$. The most stable ionization state is the trivalent one, with the $5s^2$ and $5p^6$ electrons would screen the energy levels of the 4f electrons from the effects of the surrounding environment.

Table 2.1 gives the electronic configuration of Ln^{3+} ions along with ground state and valences. As shown in table 2.1, Sc^{3+} is equivalent to Ar, Y^{3+} to Kr, and La^{3+} to Xe in electronic configuration. The lanthanides from Ce^{3+} to Lu^{3+} have one to fourteen 4f electrons added to their inner shell configuration, which is equivalent to Xe. Ions with no 4f electrons, i.e., Sc^{3+}, Y^{3+}, La^{3+}, and Lu^{3+}, have no electronic energy levels that can induce excitation and luminescence processes in or near the visible region. In contrast, the ions from Ce^{3+} to Yb^{3+}, which have partially filled 4f orbitals, have energy levels characteristic of each ion, and show a variety of luminescence properties around the visible region.

Table. 2.1 Electronic configuration of trivalent rare earth with ground states.

Atomic number	Ions	Electronic configurations	4f electron							S= $\sum m_s$	S= $\sum l_z$	J= L+S
21	Sc^{3+}	Ar								0	0	0
39	Y^{3+}	Kr								0	0	0
57	La^{3+}									0	0	0
58	Ce^{3+}	Xe	↑							1/2	3	5/2
59	Or^{3+}	Xe	↑	↑						1	5	4
60	Nd^{3+}	Xe	↑	↑	↑					3/2	6	9/2
61	Pm^{3+}	Xe	↑	↑	↑	↑				2	6	4
62	Sm^{3+}	Xe	↑	↑	↑	↑	↑			5/2	5	5/2
63	Eu^{3+}	Xe	↑	↑	↑	↑	↑	↑		3	3	0
64	Gd^{3+}	Xe	↑	↑	↑	↑	↑	↑	↑	7/2	0	7/2
65	Tb^{3+}	Xe	⇅	↑	↑	↑	↑	↑	↑	3	3	6
66	Dy^{3+}	Xe	⇅	⇅	↑	↑	↑	↑	↑	5/2	5	15/2
67	Ho^{3+}	Xe	⇅	⇅	⇅	↑	↑	↑	↑	2	6	8
68	Er^{3+}	Xe	⇅	⇅	⇅	⇅	↑	↑	↑	3/2	6	15/2
69	Tm^{3+}	Xe	⇅	⇅	⇅	⇅	⇅	↑	↑	1	5	6
70	Yb^{3+}	Xe	⇅	⇅	⇅	⇅	⇅	⇅	↑	1/2	3	7/2
71	Lu^{3+}	Xe	⇅	⇅	⇅	⇅	⇅	⇅	⇅	0	0	0

2.2.2 Luminescent properties of rare earth ions

The 4f electronic energy levels of rare earth ions are characteristic of each ion. The rare earth ions are characterized by an incompletely filled 4f shell. The 4f orbital lies inside the ion and is shielded from the surroundings by the filled $5s^2$ and $5p^6$ orbitals. Therefore, the influence of the host lattice on the optical transitions within the $4f^n$ configuration is small.

The energy levels of the trivalent rare earth ions which arise from the $4f^n$ configuration are given in Fig. 2.4. In a configurational coordinate diagram, these levels appear as parallel parabolas ($\Delta R = 0$), because the 4f electrons are well shielded from the surroundings. Emission transitions yield, therefore, sharp lines in the spectra. Since the parity does not change in such a transition, the lifetime of the excited state is long (~ 10^{-3}s).

The energy levels presented in Fig. 2.4 are split by the crystal field. The splitting is very small due to the shielding by the $5s^2$ and $5p^6$ electrons: whereas the crystal field strength in case of transition metal ions (d^n) is characteristically a few times 10000 cm^{-1}, it amounts in the rare earth ions (f^n) a few times 100 cm^{-1}.

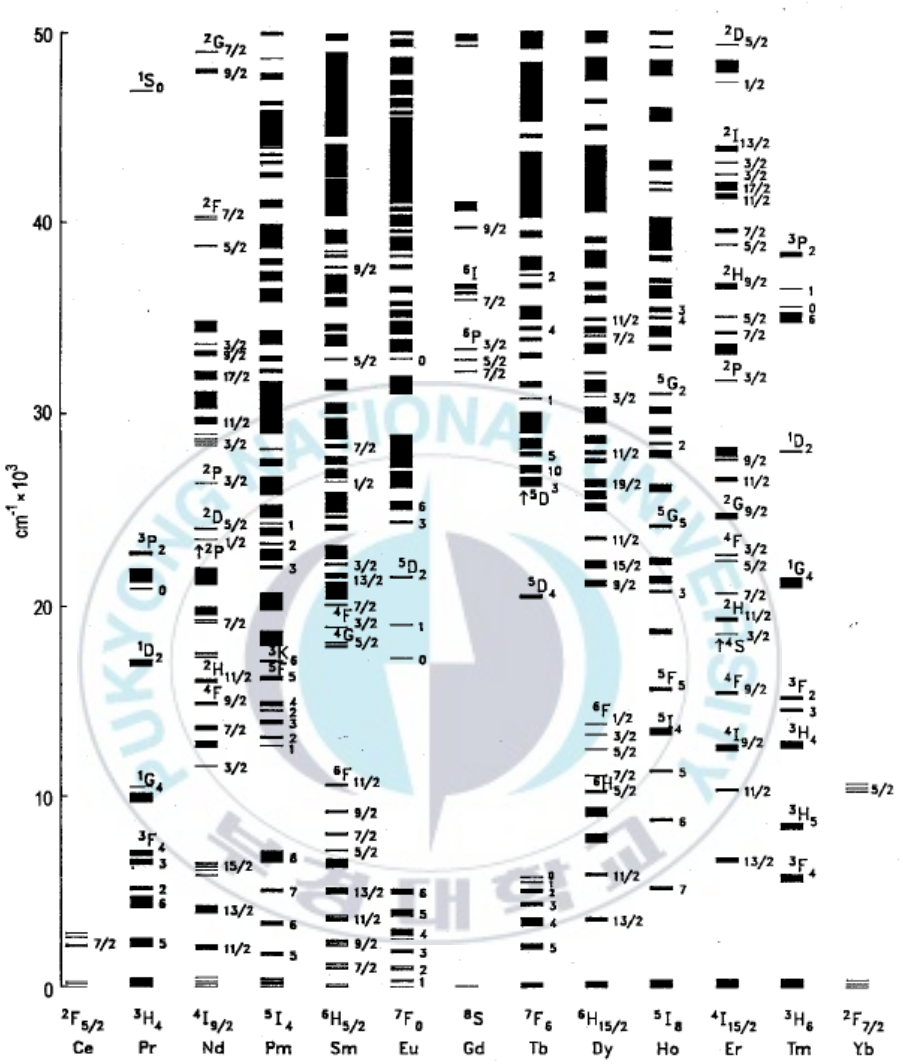

Fig. 2.4 Energy levels of the $4f^n$ configurations of the trivalent lanthanide ions

2.3 Crystal structure of $Sr_9La(PO_4)_7$

Many phosphates with whitlockite crystal structure fabricated with $M_9R(PO_4)_7$ compounds (M= Ca or Sr and R= La, y, Sc, Gd, or Bi) are applicable as host materials [13]. Specifically, such phosphate compounds have good thermal stability and have complete charge stabilization permitted by the rigid tetrahedral matrix of phosphate. Besides, they can be synthesized in an easy and inexpensive way. Currently, the luminescence of rare earth ion-doped whitlockite-type phosphates has been intensively studied in many compounds [14, 15].

The $Sr_9La(PO_4)_7$ crystallize has a rhombohedral structure with space group $R\bar{3}m$, a = b = 5.386, c = 19.827, and V = 498.057. The crystal structure of $Sr_9La(PO_4)_7$ was given in Fig. 2.5. The Sr^{2+} and La^{3+} ions share the same crystalline sites, and there are two different cation sites of Sr^{2+}/La^{3+} [21]. One ion is six oxygen coordination, and the other ion is ten oxygen coordination. Atomic coordinates and equivalent isotropic displacement parameters for compounds $Sr_9La(PO_4)_7$ are listed in Table 2.1.

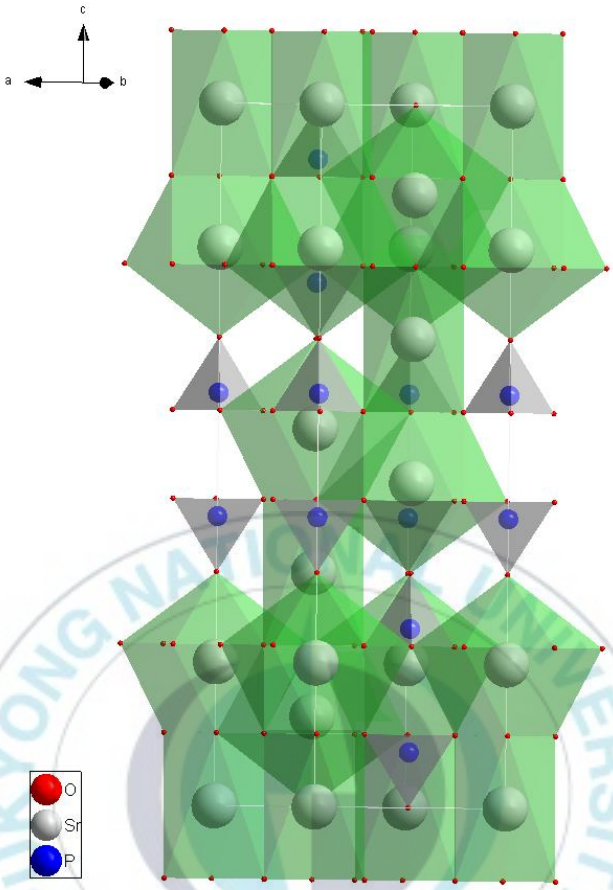

Fig. 2.5 Crystal structure of $Sr_9La(PO_4)_7$.

Table 2.2 Atomic coordinates and equivalent isotropic displacement parameters for compounds $Sr_9La(PO_4)_7$.

Atom	OX	Site	X	Y	Z
Sr1	2	3a	0	0	0
Sr2	2	6c	0	0	0.205
P	5	6c	0	0	0.412
O1	-2	6c	0	0	0.333
O2	-2	18h	0.491	0.509	0.230

OX: Oxidation states, Site: the assigned occupation site.

2.4 Luminescence properties of Tb^{3+} and Sm^{3+} in phosphor

Luminescence spectra of Tb^{3+} ion consists of many lines due to $^5D_I \rightarrow {}^7F_J$ (I= 3, 4; J= 6, 5, 4, 3, 2, 1) electronic transitions. Tb^{3+} ion has broad absorption bands in the 200-300 nm by the $4f^8 \rightarrow 4f^7 5d^1$ transition and has the narrow absorption peaks in the 300-400 nm by the $4f^8 \rightarrow 4f^8$ transitions. The emission of Tb^{3+} is due to transitions $^5D_4$ - ^7F_J, which are mainly in the green. Often there is a considerable contribution to the emission from the higher-level emission $^5D_3$ - ^7F_J, mainly in the blue. With increasing Tb^{3+} concentrations, the cross-relaxation effect occurs in $^5D_3$ – ^7F_J and $^5D_4$ - ^7F_J. As the amount of Tb^{3+} ion was increased, the following cross-relaxation process occurs [22].

$$Tb^{3+}(\,^5D_3\,) + Tb^{3+}(\,^7F_6\,) \rightarrow Tb^{3+}(\,^5D_4\,) + Tb^{3+}(\,^7F_0\,) \qquad (1)$$

The cross-relaxation reduces the blue transition of $^5D_3$ - ^7F_J and increases the green transition of $^5D_4$ - ^7F_J. In Fig. 2.6, the schematic diagram for the cross-relaxation presented. Among the emission lines from the $^5D_4$ state, the $^5D_4 \rightarrow {}^7F_5$ emission line at approximately 550 nm is the strongest in nearly all host crystals when the Tb^{3+} concentration is a few mol% or higher. The reason is that this transition has the largest probability for both electric-dipole and magnetic –dipole induced transitions.

Red and orange-red emitting phosphors can be realized by doping lanthanides with Eu^{3+} or Sm^{3+} ions and exploiting 4f $\rightarrow$ 4f transitions. However, Eu^{3+} doped phosphors display efficient luminescence only under n-UV excitation, which

limits their application in w-LEDs. While Sm^{3+} doped phosphors can be more easily stimulated by blue region radiation. Moreover, the emission of Sm^{3+} is situated in the orange-red spectral region and consists of transitions from the $^4G_{5/2}$ level to the ground state $^6H_{5/2}$ and higher levels ^6H_J (J > 5/2).

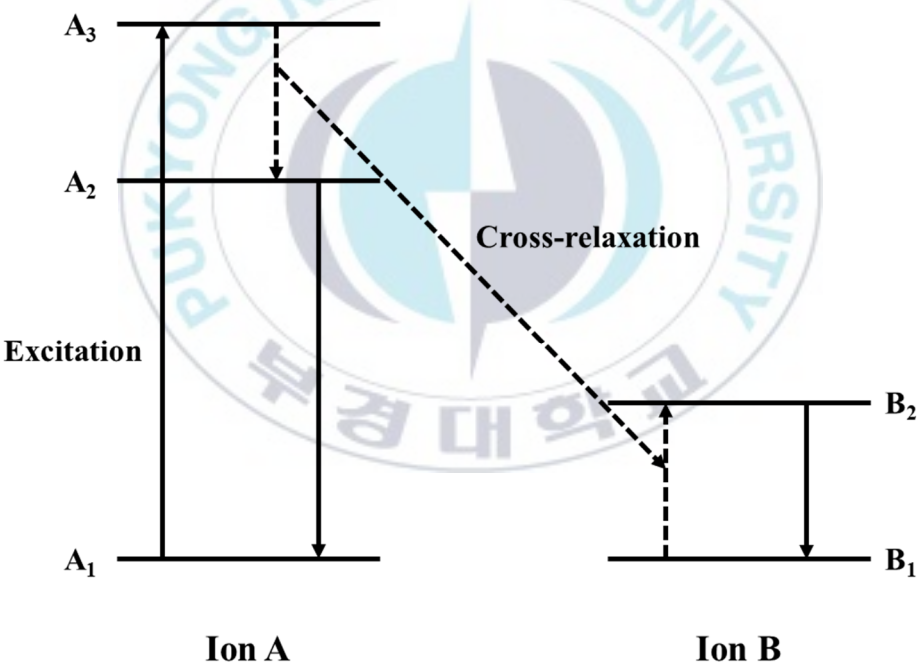

Fig. 2.6 Schematic diagram of the cross-relaxation.

. Experiment and characterization

3.1 $Sr_9La(PO_4)_7$: RE^{3+} (RE= Sm^{3+}, Tb^{3+}) phosphors synthesis method

Fig. 3.1 shows the schematic diagram of the sample preparation procedure. The samples with the formula of $Sr_9La(PO_4)_7$: RE^{3+} (RE= Sm^{3+}, Tb^{3+}) were prepared by the solid-state reaction method. The $Sr_9La(PO_4)_7$: xSm^{3+} was prepared with various Sm^{3+} concentrations from 3 to 18 mol% and the $Sr_9La(PO_4)_7$: xTb^{3+} was prepared with various Tb^{3+} concentrations from 20 to 100 mol%.

$SrCO_3$ (99.995%), La_2O_3 (99.99%), $(NH_4)_2HPO_4$ (99.9%) and Tb_4O_7 (99.9%) were thoroughly mixed by grinding. The grounded mixture of starting materials filled in the crucible was preheated at 600°C for 2h to decompose the starting reagents. After cooling down to room temperature, the preheated mixture was ground to improve the homogeneity and heated again at 1300°C for 4h.

$SrCO_3$ (99.995%), La_2O_3 (99.99%), $(NH_4)_2HPO_4$ (99.9%) and Sm_2O_3 (99.9%) were thoroughly mixed by grinding. The ground mixture of starting materials filled in the crucible was preheated at 600°C for 2h to decompose the starting reagents. After cooling down to room temperature, the preheated mixture was ground to improve the homogeneity and heated again at 1300°C for 4h.

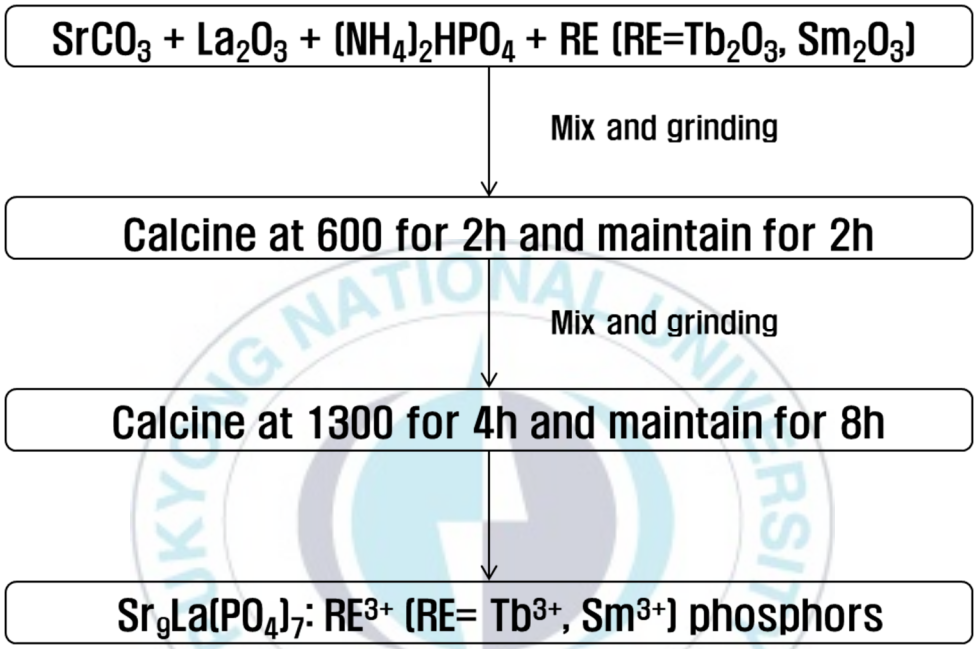

Fig. 3.1 A schematic diagram of processing steps involved in the synthesis of $Sr_9La(PO_4)_7$: RE^{3+} ($RE= Sm^{3+}$, Tb^{3+})

3.2 characterization and optical measurements

The phase of all samples verified by using powder X-ray diffraction (XRD). The XRD profiles measured within the range of $10 - 80°$ in steps of $0.02°$ using a Philips X'Pert multipurpose diffractometer (Philips, Netherlands) with Cu K_α radiation as shown in Fig. 3.2. The photoluminescence (PL) and photoluminescence excitation (PLE) spectra and decay time measured by using a Photon Technology International Fluorimeter (PTI, USA) with a 60W Xe-arc lamp as the excitation light source.

Fig. 3.2 X-ray diffractometer (X'Pert MPD, Philips)

. Results and Discussions

4.1 Luminescence properties of Sm^{3+} doped $Sr_9La(PO_4)_7$ phosphor

4.1.1 Phase characterization and crystal structure

Fig. 4.1 shows the XRD patterns of prepared $Sr_9La(PO_4)_7$: xSm^{3+} (x= 0.01, 0.03, 0.06, 0.09, 0.12). Considering the effective radii of Sm^{3+} ions, the Sm^{3+} ions were expected to occupy the La^{3+} ion site in the $Sr_9La(PO_4)_7$ crystals. All XRD patterns can be well fitted with the standard patterns of the $Sr_3(PO_4)_2$ (PDF #024-1008) belonging to the rhombohedral crystal system, with a space group of $R\bar{3}m$ (166). The doped Sm^{3+} ions do not affect the crystal lattice of $Sr_9La(PO_4)_7$. This suggests that all samples are crystallized in the single phase.

To further confirm identify the influence of Sm^{3+} ions on the crystal structure, Rietveld refinement of the optimal concentration of the sample was performed. The initial structural model for Rietveld refinement was constructed based on the $Sr_3(PO_4)_2$ structure. Fig. 4.2 shows Rietveld refinement results on the optimized concentration x = 0.03 using the software General Structure Analysis System (GSAS). The parameters obtained from the refinement data were R_{wp} = 9.18% and R_p = 5.94%. The detailed parameters of the Rietveld refinement of the host and $Sr_9La(PO_4)_7$: $0.03Sm^{3+}$ sample are listed in Table 4.1. By comparison, it is shown that the cell volume of $Sr_9La(PO_4)_7$: $0.03Sm^{3+}$ is smaller than that of $Sr_9La(PO_4)_7$. The replacement of the larger Sr^{2+} (CN= 6, R= 1.18) ions by smaller Sm^{3+} (CN= 6, R= 0.958) resulted in the reduction of the parameters.

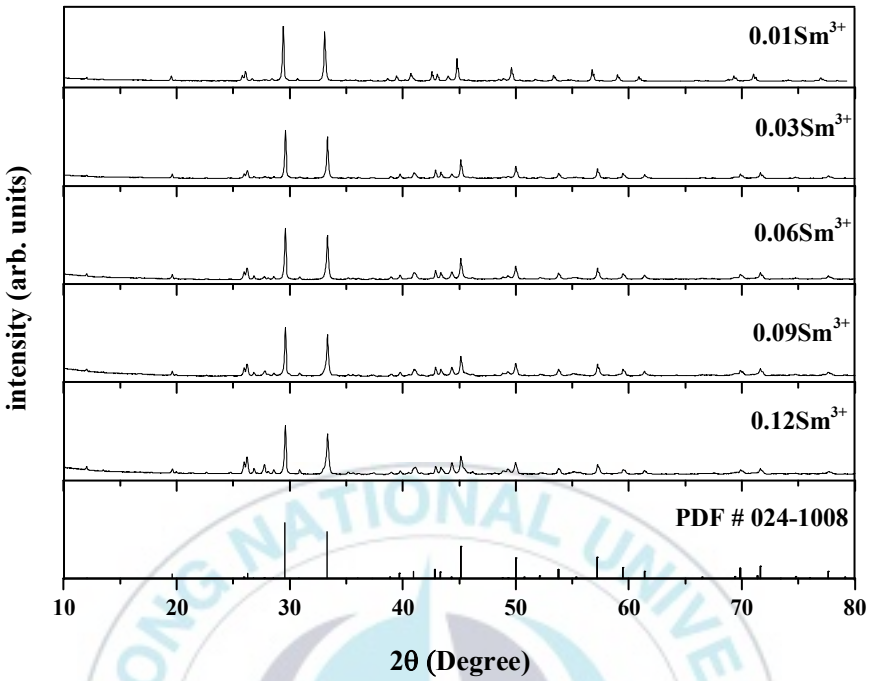

Fig. 4.1 The XRD patterns of $Sr_9La(PO_4)_7$: xSm^{3+} (x= 0.01, 0.03, 0.06, 0.09, 0.12) and standard reference.

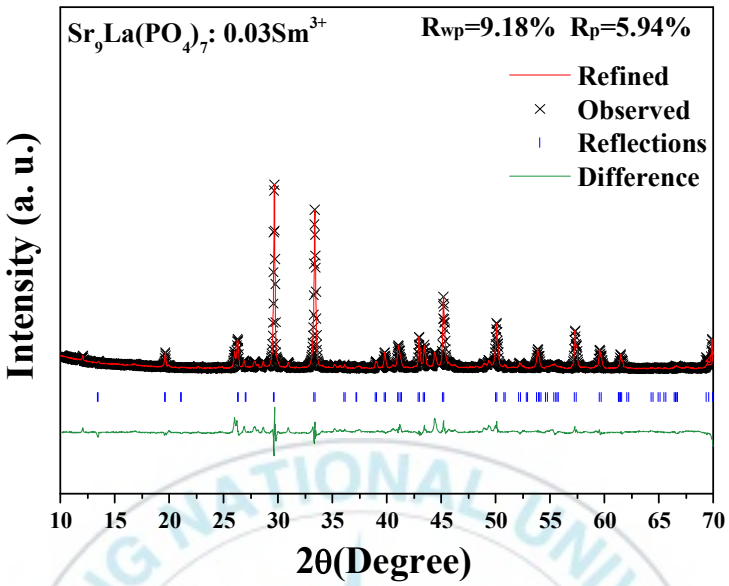

Fig. 4.2 Rietveld refinement of XRD patterns of $Sr_9La(PO_4)_7$: $0.03Sm^{3+}$.

Table 4.1 The refinement parameters of $Sr_9La(PO_4)_7$: $0.03Sm^{3+}$.

Compound	$Sr_9La(PO_4)_7$	$Sr_9La(PO_4)_7$: $0.03Sm^{3+}$
Space group	$R\bar{3}m$ (166)	$R\bar{3}m$ (166)
a (Å)	5.386	5.377
b (Å)	5.386	5.377
c (Å)	19.827	19.812
V (Å^3)	498.057	496.15
α(˚)	90	90
β(˚)	90	90
γ(˚)	120	120
R_{wp}(%)	6.52	9.18
R_p(%)	4.66	5.94

Fig. 4.3(a) and (b) show the unit cell crystal structure of $Sr_9La(PO_4)_7$: xSm^{3+} (x= 0.03) and the two kinds of different coordination environments of the cation sites, respectively. In the crystal structure, due to the similar valence and ionic radii, the Sr^{2+} and La^{3+} ions are located at the same crystalline sites. The Sr^{2+}/La^{3+} ions are distributed between two crystallographic sites. Sr_1/La_1 and Sr_2/La_2 are coordinated with six and ten oxygen atoms, respectively.

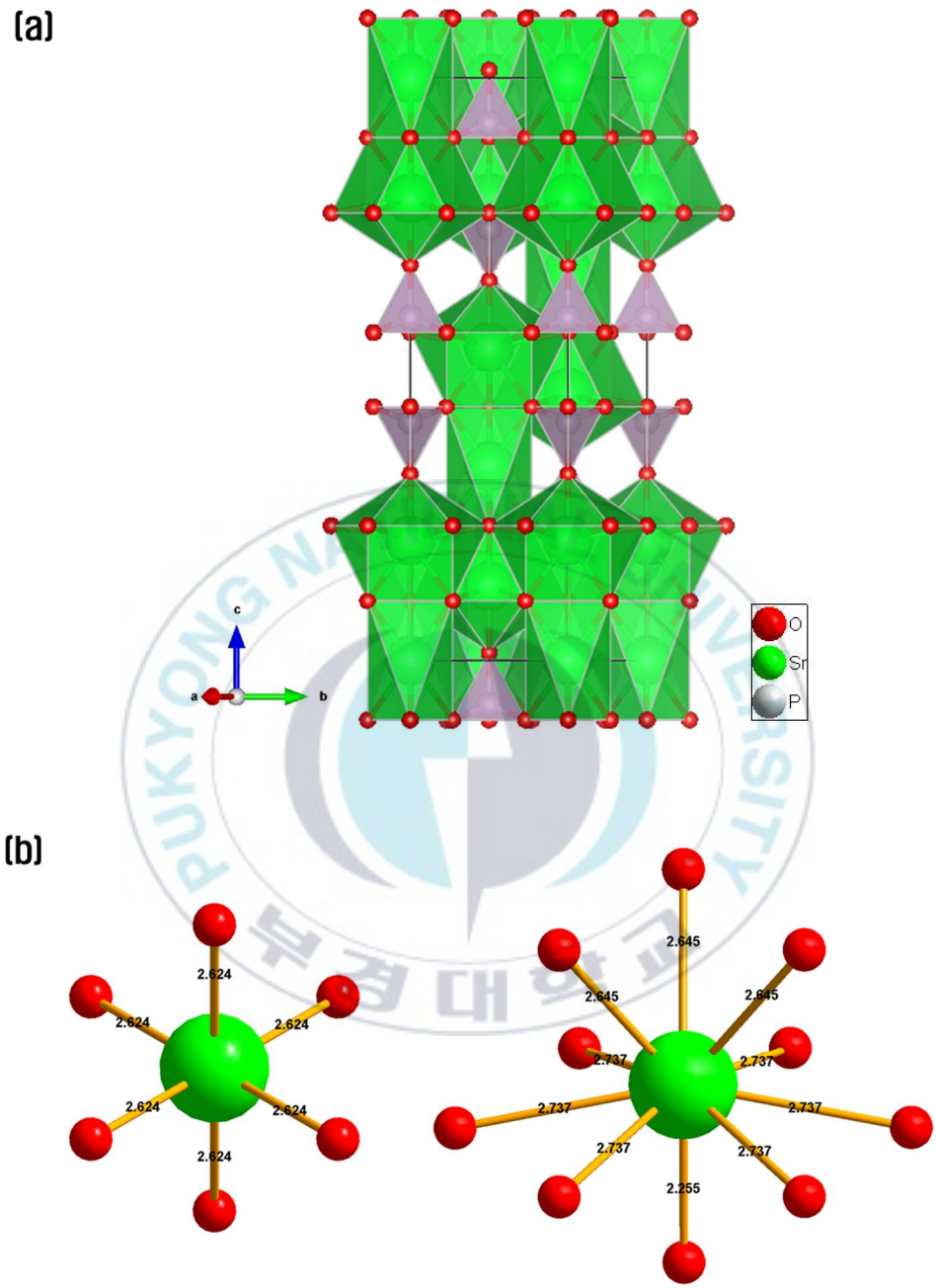

Fig. 4.3 (a) Crystal structure of $Sr_9La(PO_4)_7$: $0.03Sm^{3+}$. (b) Coordination environment of Sm^{3+} sites.

4.1.2 Photoluminescence properties

Fig. 4.4 (a) shows the PLE spectra of the $Sr_9La(PO_4)_7$: xSm^{3+} (x= 0.01, 0.03, 0.06, 0.09, 0.12) phosphors monitored at 595 nm. All PLE spectra have narrow absorption peaks in the wavelength range from 300 to 500 nm, which were corresponding to the 4f-4f transition of Sm^{3+} ions [23–25]. The observed peaks around 341, 358, 370, 398, 413, 436 and 467 nm, corresponds to the transition from ground state level $^6H_{5/2}$ to the excited state levels $^4H_{9/2}$, $^4D_{3/2}$, $^6P_{7/2}$, $^4H_{7/2}$, $^4L_{13/2}$, $^4G_{9/2}$ and $^4I_{11/2}$ of Sm^{3+} ions. Among this transition, the most intense band is located at 399 nm. Fig. 4.4 (b) shows the PL spectra of the $Sr_9La(PO_4)_7$: xSm^{3+} (x= 0.01, 0.03, 0.06, 0.09, 0.12) phosphors monitored at 399 nm. All PL spectra indicate the four typical emission peaks of Sm^{3+}, which associated with $^4G_{5/2} \rightarrow {}^6H_J$ (J = 5/2, 7/2, 9/2, 11/2) transitions [26, 27]. Among these transitions, the $^4G_{5/2} \rightarrow {}^6H_{7/2}$ transition was the most intense one. And according to the selection rules, this was a partially magnetic dipole (MD) and partially electric dipole (ED) transition, while $^4G_{5/2} \rightarrow {}^6H_{9/2}$, as well as $^4G_{5/2} \rightarrow {}^6H_{11/2}$, was purely ED transitions and $^4G_{5/2} \rightarrow {}^6H_{5/2}$ was purely MD transition. Generally, the intensity ratio of ED and MD transitions is a suitable index of the symmetry of the local environment of Sm^{3+} in the host. When the obtained ratio value is below 1, the characteristic of the host matrix occupies the asymmetric. Meanwhile, when the obtained ratio value is above 1, the characteristic of the host matrix occupies the symmetric.

Fig. 4.4 (c) shows the emission intensities of Sm^{3+} as a function of the doping concentrations. With the increase of Sm^{3+} ion concentration from 0.01 to 0.12 mol, the intensity of the luminescence increased until it reaches 0.03 mol and then

decreased due to the concentration quenching. This concentration quenching is due to the non-radiative energy transfer between different Sm^{3+} ions.

Energy transfer can be divided into two, one is exchanging interaction, and the other is multipole-multipole interaction. It is known that if the critical distance is shorter than 5 , the energy transfer occurs due to the exchange interaction. Meanwhile, if the critical distance is much larger than 5 , the energy transfer can be ascribed to the multipole-multipole interaction. The critical distance R_c for between Sm^{3+} ions are estimated by using the equation proposed by Blasse [28]:

$$R_c = 2\left[\frac{3V}{4\pi X_c N}\right]^{1/3} \quad (2)$$

in which V stands for the volume of the unit cell, X_c is the critical concentration of activator ion (Sm^{3+}) beyond concentration quenching, and N represents the number of host cations in on unit cell. In this case, N = 3, V was estimated to be 496.15 , and X_c is 0.03 according to the above discussions. According to the equation, R_c was turned to 21.917 . Therefore, the energy transfer mechanism of concentration quenching of Sm^{3+} in $Sr_9La(PO_4)_7$ phosphor is the multipole-multipole interaction because the critical distance the calculated of Sm^{3+} doped phosphor is much larger than 5 .

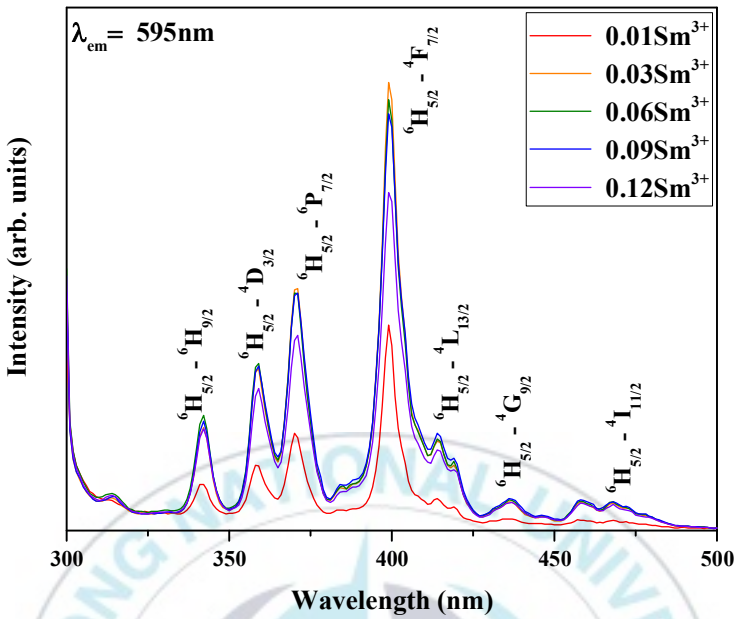
λem= 595nm
0.01Sm3+
0.03Sm3+
0.06Sm3+
0.09Sm3+
0.12Sm3+
6H5/2 - 6H9/2
6H5/2 - 4D3/2
6H5/2 - 6P7/2
6H5/2 - 4F7/2
6H5/2 - 4L13/2
6H5/2 - 4G9/2
6H5/2 - 4I11/2
Intensity (arb. units)
300
350
400
450
500
Wavelength (nm)

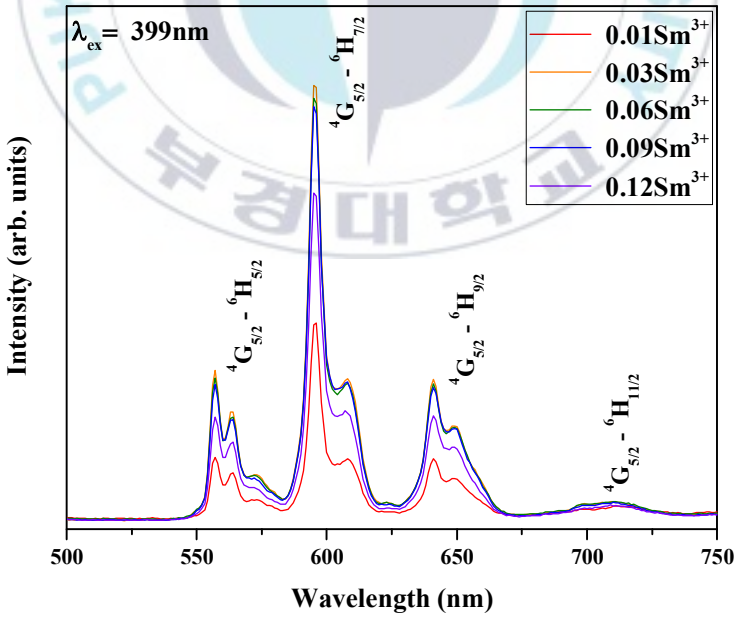
λex= 399nm
0.01Sm3+
0.03Sm3+
0.06Sm3+
0.09Sm3+
0.12Sm3+
4G5/2 - 6H5/2
4G5/2 - 6H7/2
4G5/2 - 6H9/2
4G5/2 - 6H11/2
Intensity (arb. units)
500
550
600
650
700
750
Wavelength (nm)

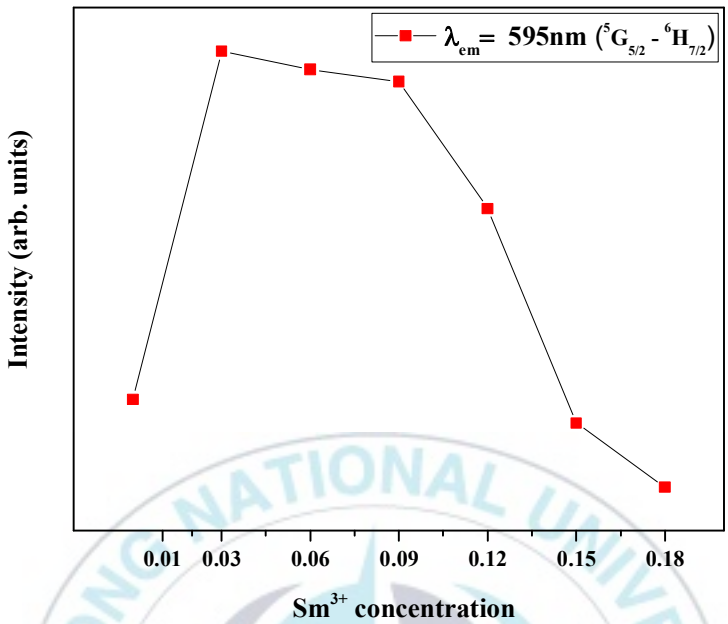

Fig. 4.4 (a) PL excitation spectra monitored at 595 nm. (b) PL spectra monitored at 398 nm. (c) The dependence of emission intensities on Sm^{3+} concentrations.

Based on the analysis above, we know that electric multipole-multipole interaction plays a leading role in this quenching process. On the basis of Van Uitert equation, the mechanism of interaction between Sm^{3+} follows the formula below [29]:

$$\frac{1}{x} = K\left[1 + \beta(x)^{\theta/3}\right]^{-1} \tag{3}$$

where x refers to the concentration of Sm^{3+}, K and $\beta(x)$ are constant for the same excitation conditions for a given host crystal. $\theta = 6$, 8 and 10 are dipole–dipole, dipole–quadrupole and quadrupole–quadrupole interactions, respectively. As we know the electric multipolar character can be determined by the slope ($\theta/3$) which calculated by equation (3). Fig. 4.5 exhibits the dependence of log (I/x)/log x which can fit as a line with the slope $(\theta/3) = -1.16$. Therefore, the value of θ is calculated 3.48, which is close to 6 approximately, indicating that the dominant interaction for the cross relaxation of the $^4G_{5/2}$ is dipole-dipole interaction.

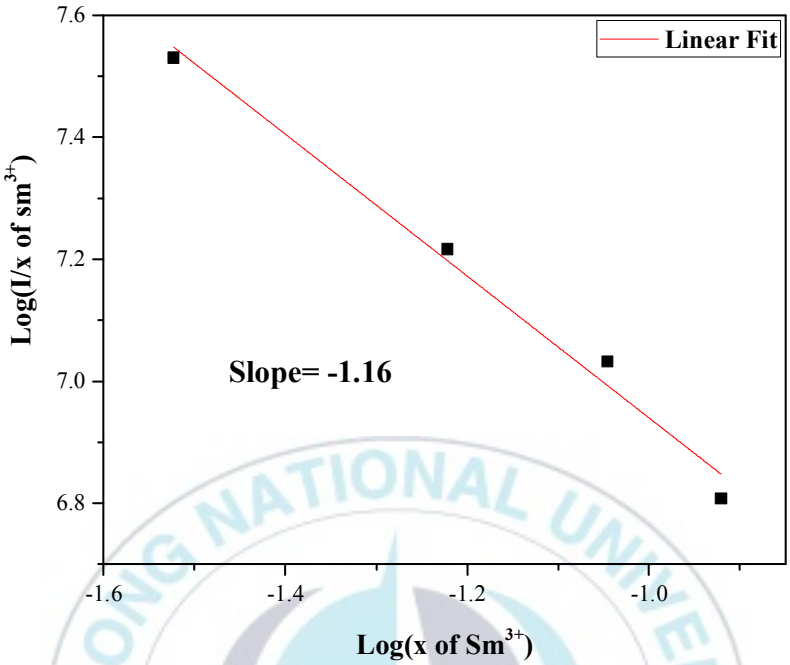

Fig. 4.5 Curve of log I/x vs. log x in $Sr_9La(PO_4)_7$: xSm^{3+} phosphor (λ_{ex}= 399nm).

To further investigate luminescence properties, Fig. 4.6 shows the fluorescence decay curves of $Sr_9La(PO_4)_7$: xSm^{3+} phosphors (x= 0.01, 0.03, 0.06, 0.09, 0.12) under 399 nm excitation and monitored at 595 nm. Each curve exhibited a double exponential decay and could be calculated by the following equation [30]:

$$I(\tau) = A_1\, exp\left(\frac{-t}{\tau_1}\right) + A_2\, exp\left(\frac{-t}{\tau_2}\right) \qquad (4)$$

Where I(τ) is the luminescence intensities at time τ_1 and τ_2, respectively, and A_1 and A_2 are a constants τ_1 and τ_2 are the decay times for the exponential components. The detailed fitting parameters of different decay curves are shown in Table 4.2. The lifetimes of Sm^{3+} monitored at 595 nm resulting from the equation, were 4.16, 6.45, 8.30, 9.51, and 13.22 μs. There is an increasing trend in the lifetime with an increasing Sm^{3+} concentration. Indeed, this difference is interesting and worth further investigation.

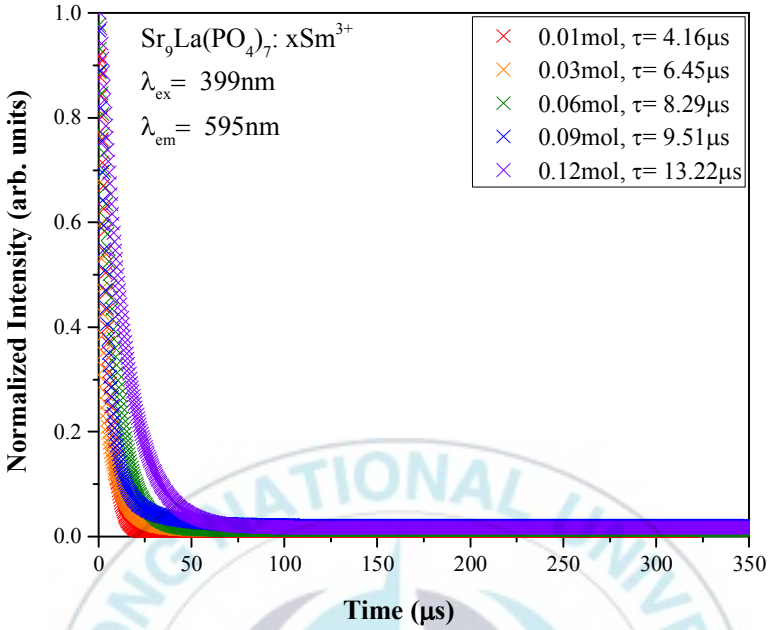

Fig. 4.12 Decay curves of $Sr_9La(PO_4)_7$: xSm^{3+} (x= 0.01, 0.03, 0.06, 0.09, 0.12).

Table 4.2 Fitting parameters of different decay curves for $Sr_9La(PO_4)_7$: xSm^{3+}.

Samples	A_1	τ_1(μs)	A_2	τ_2(μs)	τ(μs)
x= 0.01	1.43	3.82	-0.52	1.24	4.16
x= 0.03	0.71	1.65	0.30	8.66	6.45
x= 0.06	0.31	8.30	0.70	8.30	8.30
x= 0.09	0.93	4.30	0.11	19.58	9.51
x= 0.12	0.36	13.22	0.68	13.22	13.22

For a better understanding of the luminescence behaviors of Sm^{3+} in $Sr_9La(PO_4)_7$, the energy level diagram of Sm^{3+} was shown in Fig. 4.7. The Sm^{3+} ions are excited from the $^6H_{5/2}$ to the $^4F_{7/2}$ when the sample is irradiated by 398 nm light. The states were relaxed to the $^4G_{5/2}$ by non-radiative (NR) transitions due to smaller energy differences between excited state levels. As a result, four emission peaks can be observed corresponding to the $^4G_{5/2}$ to ^6H_J (J= 5/2, 7/2, 9/2, 11/2) emission of Sm^{3+}.

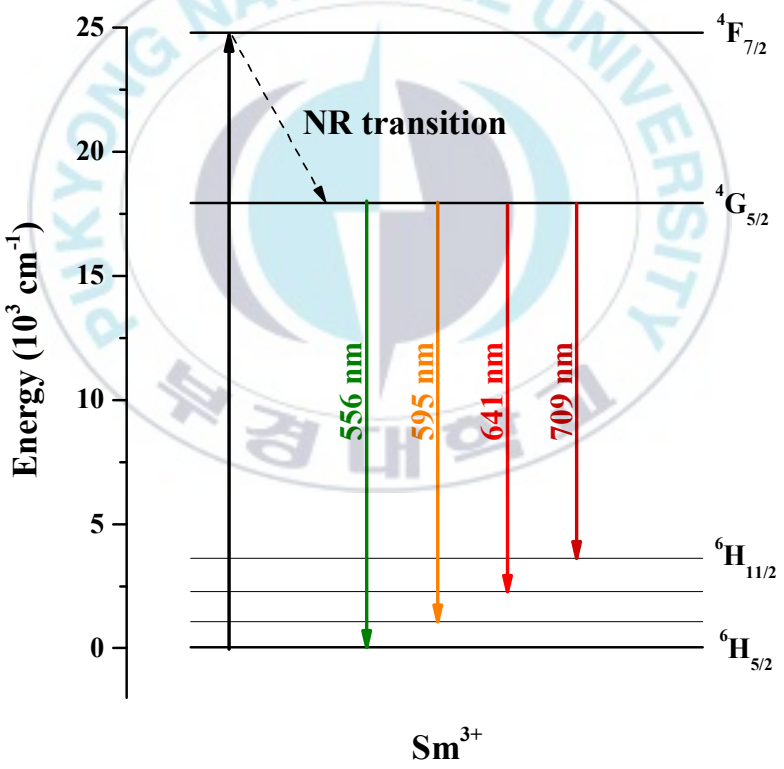

Fig. 4.13 Sm^{3+} energy level diagram.

4.2 Luminescence properties of Tb^{3+} doped $Sr_9La(PO_4)_7$ phosphor

4.2.1 Phase characterization and crystal structure

The XRD patterns of $Sr_9La_{1-x}(PO_4)_7$: xTb^{3+} (x= 0, 0.2, 0.4, 0.6, 0.8, 1) phosphors are shown in Fig. 4.8(a). The diffraction peaks of the synthesized samples corresponding to the host and Tb^{3+} doped phosphors were consistent with those of JCPDS No. 024-1008 and 054-1185, respectively. However, for all the Tb^{3+} doped samples, one additional weak diffraction peak at 27.9° denoted due to the impurity. The magnified XRD patterns in the region of 32.8-34° are shown in Fig. 4.8(b). It is observed that the second main peak decreases and shifts as the concentration of Tb^{3+} increases from 0.4 mol to 0.6 mol. These results imply that the host lattice structure changes by the doping Tb^{3+} ion.

To further confirm the variation of crystal structure, the software General Structure Analysis System (GSAS) was used for Rietveld refinement on the basis of XRD patterns. Fig. 4.9 (a) and (b) shows the Rietveld refinement results for the $Sr_9La(PO_4)_7$ (host) and $Sr_9Tb(PO_4)_7$ (x= 1). The results indicate that the phosphors of a whitlockite-type structure have been made, and the crystal structure has changed by doping Tb^{3+} ions. The refinement parameters of $Sr_9La_{1-x}(PO_4)_7$: xTb^{3+} (x= 0, 1) are listed in Table. 4.3. The crystal structure of the host is rhombohedral with a space group of $R\bar{3}m$ and cell parameters of a = b = 5.3887, c = 19.795, and V = 497.797. The crystal structure of Tb^{3+}-doped phosphors is monoclinic with a space group of I2/a and cell parameters of a = 18.038, b = 10.640, c = 18.474, V = 2590.81, and Z = 4.

Fig. 4.10 shows the crystal structure of the compound of the Rietveld refinement

results. Fig. 4.10 (a) shows the crystal structure of the host lattice viewed along the a* direction in the parallel projection. The Sr^{2+} and La^{3+} ions share the same crystalline sites, and there are two different cation sites of Sr^{2+}/La^{3+}. Fig. 4.10 (b) shows the crystal structure of $Sr_9Tb(PO_4)_7$ viewed along the b direction in the parallel projection. There are five different cation sites of Sr^{2+}. The La^{3+} ion site has only one cation site. Also, the doped Tb^{3+} ions are replaced by La^{3+} ions due to their similar valence and ionic radii. Fig. 4.10 (c) shows the cation site occupied by Tb^{3+}. The terbium ions are surrounded by $[PO_4]^{3-}$ tetrahedrons. Also, the shortest Tb-Tb distances in $Sr_9Tb(PO_4)_7$ is about 9.019 , which is the long distance that the energy migration of the doped rare earth ions is difficult.

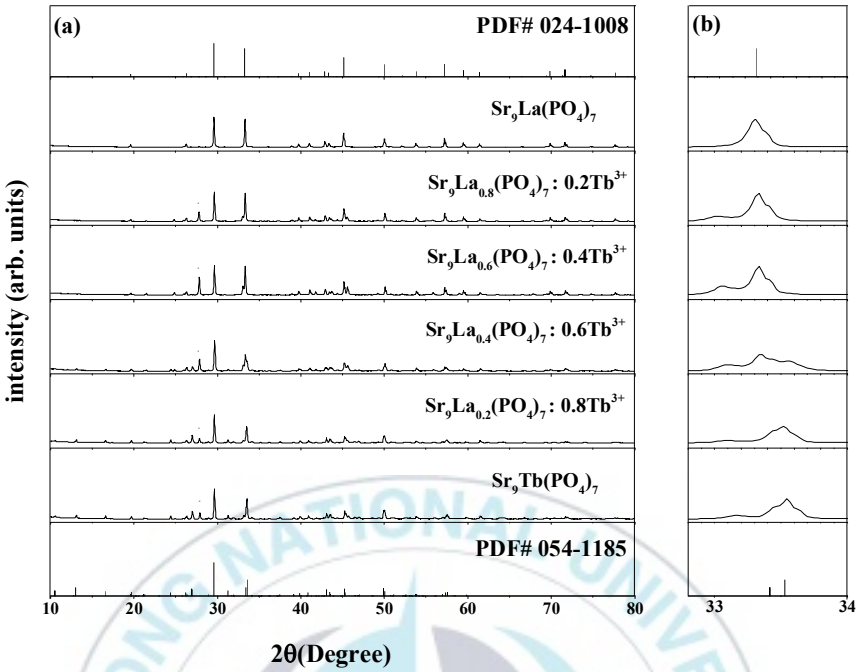

Fig. 4.8 (a) The XRD patterns of $Sr_9La_{1-x}(PO_4)_7$: xTb^{3+} phosphor and standard references. and (b) the magnified XRD patterns in the region of 32.8-34°.

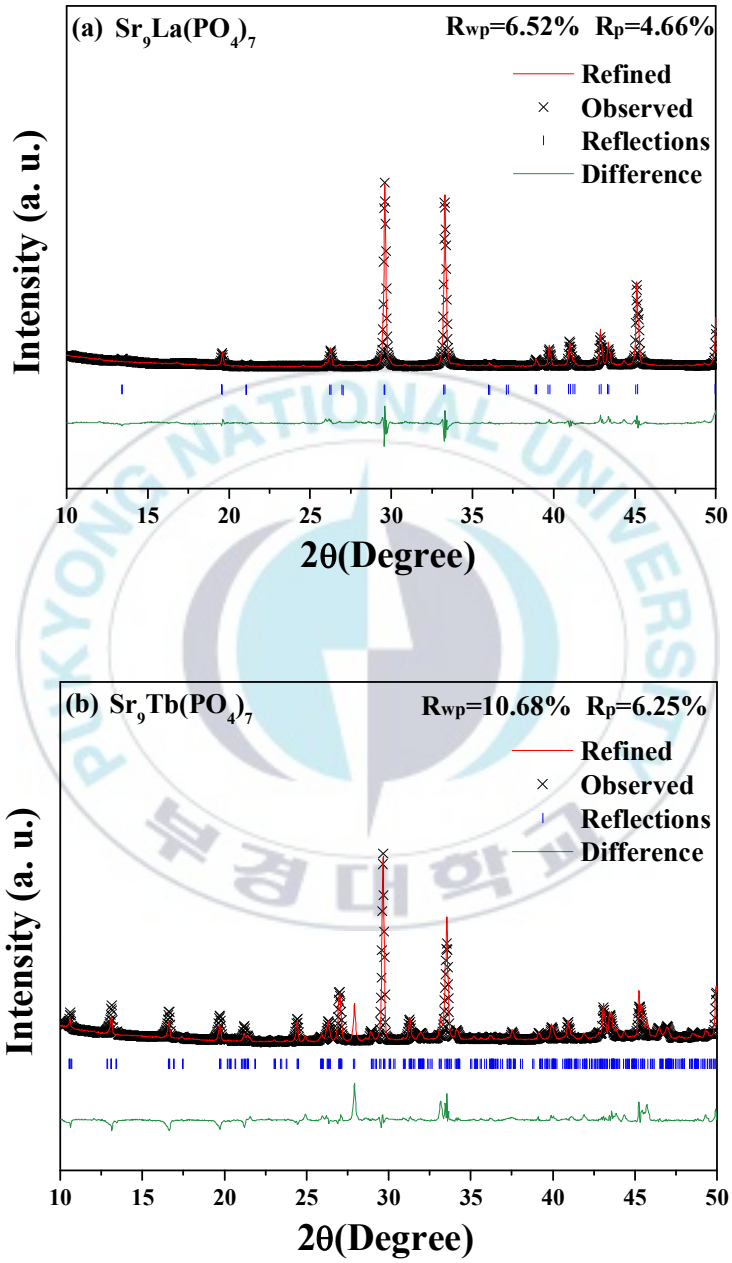

Fig. 4.9 (a) Rietveld refinement of XRD patterns of Host. (b) $Sr_9Tb(PO_4)_7$.

Table 4.3 The refinement parameters of $Sr_9La(PO_4)_7$ and $Sr_9Tb(PO_4)_7$.

Compound	$Sr_9La(PO_4)_7$	$Sr_9Tb(PO_4)_7$
Space group	$R\bar{3}m$ (166)	$I2/a$ (15)
a ( )	5.386	10.038
b ( )	5.386	10.640
c ( )	19.827	18.474
V (^{3})	498.057	2590.811
α(˚)	90	90
β(˚)	90	133.054
γ(˚)	120	90
R_{wp}(%)	6.52	10.68
R_p(%)	4.66	6.25

(a)

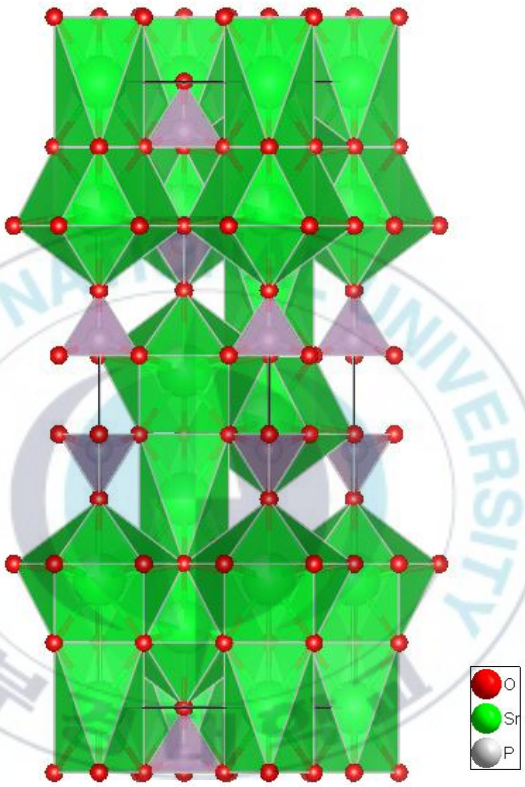

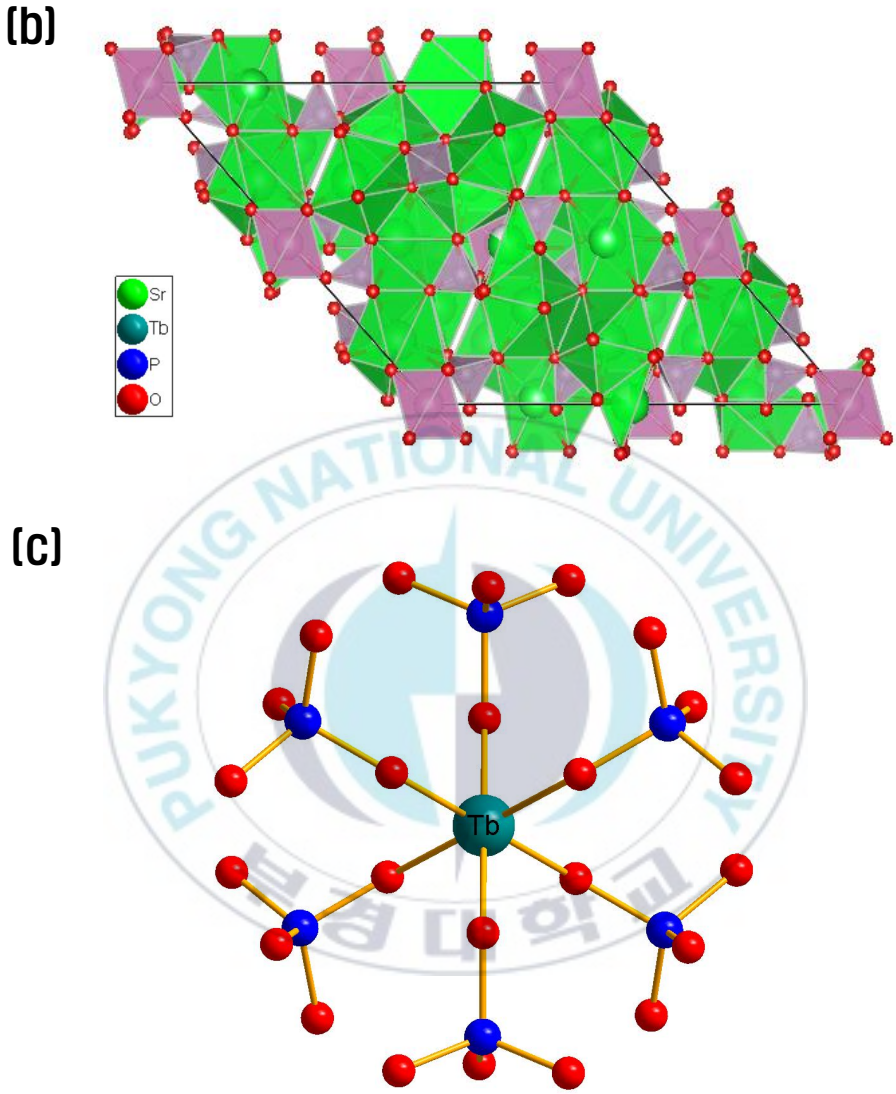

Fig. 4.10 (a) Crystal structure of $Sr_9La(PO_4)_7$. (b) Crystal structure of $Sr_9Tb(PO_4)_7$. (c) Coordination environment of Tb^{3+} site.

The fine local structure of $Sr_9La(PO_4)_7$: xTb^{3+} (x= 0.2, 1) were further examined by high resolution transmission electronic microscope (HRTEM). The HRTEM image in Fig. 4.11 shows well defined lattice fringes in various regions with agglomerated particles. The samples were chosen with x= 0.2, 1 to facilitate observation of the crystal structure. The measured lattice spacing is about 2.50 corresponding to the (015) plane, as shown in Fig. 4.11(a). This indicates that the $Sr_9La(PO_4)_7$: xTb^{3+} (x= 0.2) crystal preferred orientation growth along the (015) direction, which is consistent with the XRD results of $R\bar{3}m$. On the other hand, the lattice spacing of $Sr_9La(PO_4)_7$: xTb^{3+} (x= 1) crystal is about 3.80 corresponding to the (222) plane, which is consistent with the XRD results of I2/a, as shown in Fig. 4.11(b).

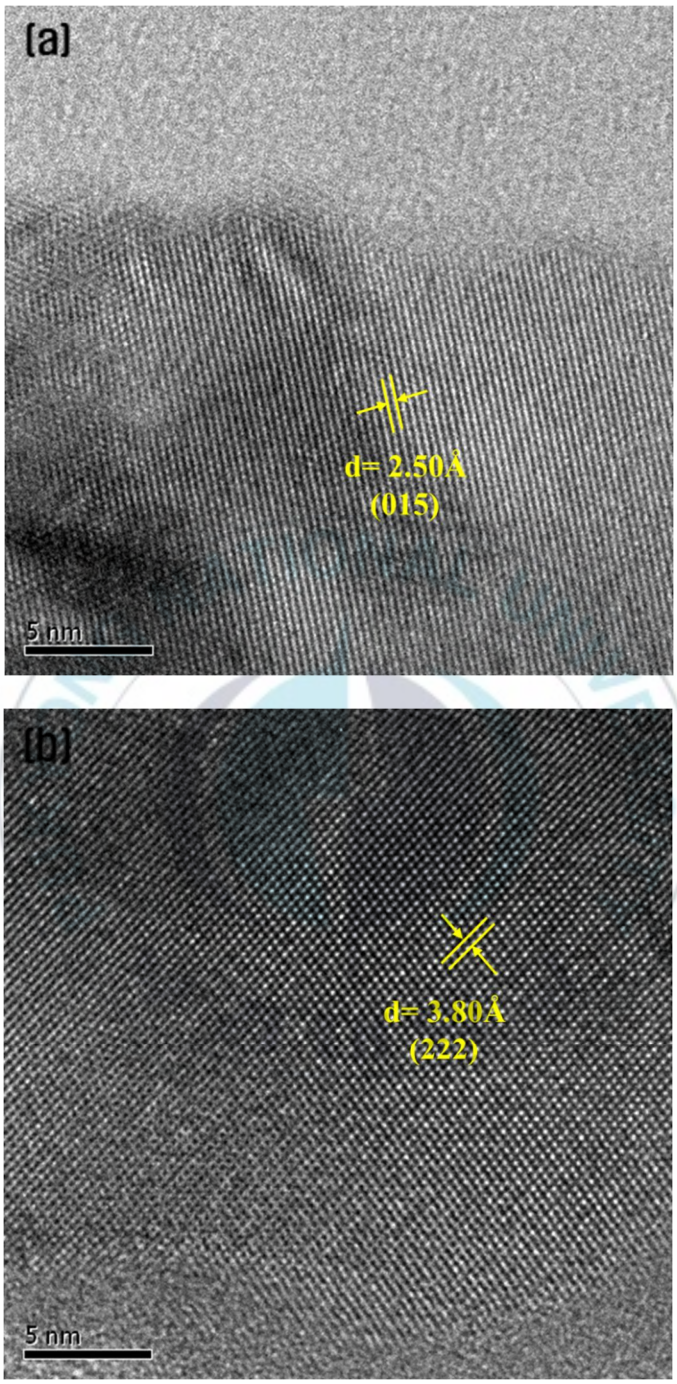

Fig. 4.11 (a) HRTEM images of $Sr_9La(PO_4)_7$: $0.2Tb^{3+}$, (b) HRTEM images of $Sr_9Tb(PO_4)_7$.

4.2.2 Photoluminescence properties

Fig. 4.12 (a) shows the PL excitation (PLE) spectrum of the $Sr_9La_{1-x}(PO_4)_7$: xTb^{3+} (x= 0, 0.2, 0.4, 0.6, 0.8, 1) phosphors monitored at 542 nm. The PLE spectrum of $Sr_9La_{1-x}(PO_4)_7$: xTb^{3+} (x = 0, 0.2, 0.4, 0.6, 0.8, 1) have a broad band of 200–300 nm with a maximum band at about 279 nm and the bands are attributed to the $4f^8$–$4f^75d^1$ transition of Tb^{3+}. The wavelength region peaks of 300–500 nm are the f–f transitions of the Tb^{3+} [31–33]. The peaks at 301, 316, 350, 376, and 481 nm are assigned to the Tb^{3+} transition of $^7F_6 \rightarrow {}^5H_6$, $^7F_6 \rightarrow {}^5H_7$, $^7F_6 \rightarrow {}^5D_2$, $^7F_6 \rightarrow {}^5G_6$, and $^7F_6 \rightarrow {}^5D_4$, respectively.

Fig. 4. 12 (b) and (c) show the emission spectra of the $Sr_9La_{1-x}(PO_4)_7$ (x= 0, 0.2, 0.4, 0.6, 0.8, 1) phosphors monitored at 376 nm and 279 nm. The peaks observed at 500, 542, 583, and 621 nm are attributed to the $^5D_4 \rightarrow {}^7F_J$ (J= 3, 4, 5, 6) transitions [34–36]. Generally, it is well known that the emission spectra of Tb^{3+} divide into two groups due to the 4f–4f transitions. One belongs to the $^5D_3$–^7F_J transition in the blue emission and the other is belong to the $^5D_4$–^7F_J (J= 6, 5, 4, 3) transition in the green emission. In particular, among these peaks, the intensity of the $^5D_4 \rightarrow {}^7F_5$ transition is a characteristic transition of Tb^{3+}. As the Tb^{3+} concentration increases, the blue emissions from the $^5D_3$–^7F_J transitions decrease progressively, while the green emissions from the $^5D_4$–^7F_J transitions increase continuously. Hence, if the Tb^{3+} concentration is sufficiently high, the emission from the $^5D_3$ level of Tb^{3+} is much weaker than the emission from the $^5D_4$ level due to the cross-relaxation through the resonant energy transfer process [37]. It is believed that these findings are consistent with the results of the emission spectrum.

The emission intensities of Tb^{3+} as a function of the doping concentrations are shown in Fig. 4.12 (d). The emission intensity of 542 nm ($^5D_4 \rightarrow {}^7F_5$) increases until the Tb^{3+} concentration reaches from x = 0.2 to x = 1.0 consistently. These results confirm that complete quenching does not occur at x = 1.0, where the La^{3+} site is completely replaced by Tb^{3+}. This is due to the structural characteristics of the $Sr_9Tb(PO_4)_7$ crystal structure. As can be seen in Fig. 4.10(c), Tb^{3+} ions occupy the polyhedral and they are separated from each other by a large spatial distance by the $[PO_4]^{3-}$ tetrahedrons. The large spatial distance between the Tb^{3+} ion and the shielding of the $[PO_4]^{3-}$ tetrahedrons interferes with the energy transfer between the Tb^{3+} ions. As a result, it prevents the occurrence of concentration quenching. Therefore, high concentration quenching was observed in $Sr_9La_{1-x}(PO_4)_7$: xTb^{3+} phosphors.

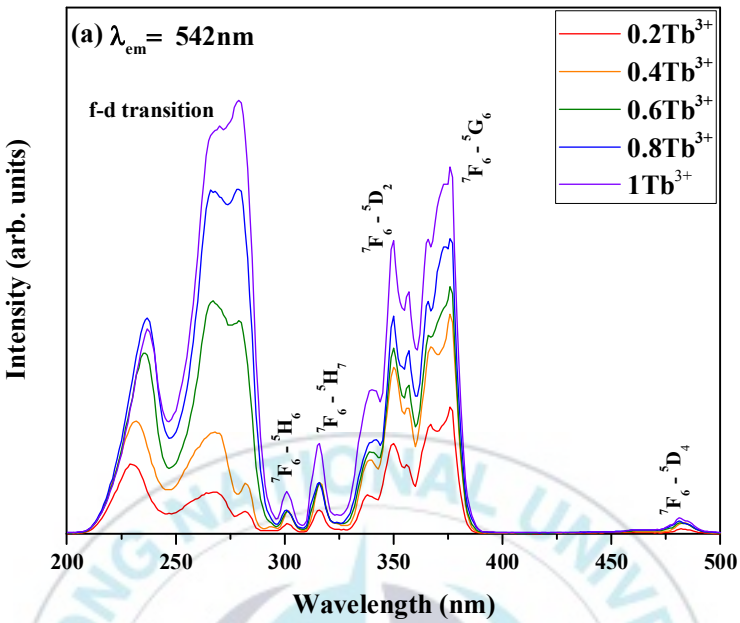
(a) λem= 542nm
f-d transition
0.2Tb3+
0.4Tb3+
0.6Tb3+
0.8Tb3+
1Tb3+
7F6 - 5H6
7F6 - 5H7
7F6 - 5D2
7F6 - 5G6
7F6 - 5D4
Intensity (arb. units)
200
250
300
350
400
450
500
Wavelength (nm)

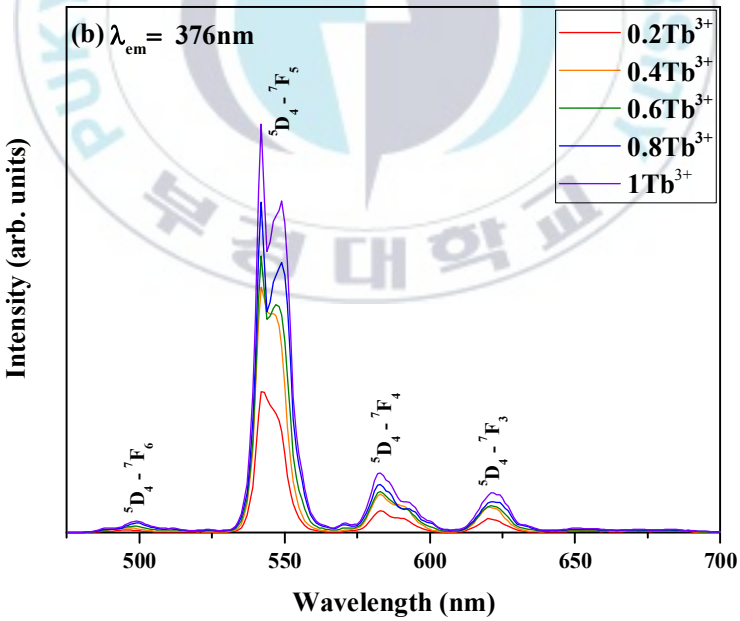
(b) λem= 376nm
0.2Tb3+
0.4Tb3+
0.6Tb3+
0.8Tb3+
1Tb3+
5D4 - 7F6
5D4 - 7F5
5D4 - 7F4
5D4 - 7F3
Intensity (arb. units)
500
550
600
650
700
Wavelength (nm)

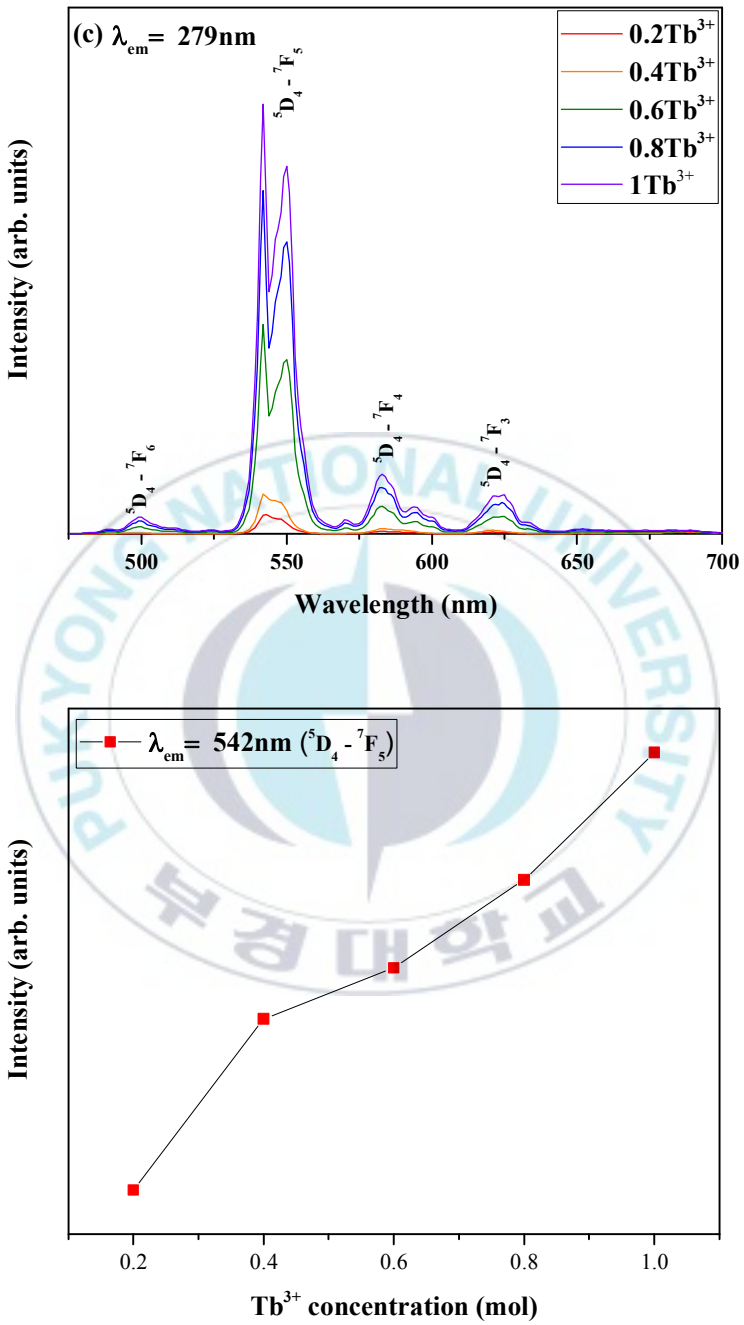

Fig. 4.12 (a) PL excitation spectra monitored at 542 nm. (b) PL spectra monitored at 376nm. (c) PL spectra monitored at 279nm. (d) The dependence of emission intensities on Tb^{3+} concentrations.

To further investigate luminescence properties, the luminescence decay curves for the green emission (542 nm) of $Sr_9La_{1-x}(PO_4)_7$: xTb^{3+} phosphors at 376 nm excitation are shown in Fig. 4.13. Decay curves were fitted by a double exponential equation defined as follows [30]:

$$I(\tau) = A_1\, exp\left(\frac{-t}{\tau_1}\right) + A_2\, exp\left(\frac{-t}{\tau_2}\right) \qquad (4)$$

Where $I(\tau)$ is the luminescence intensities at time τ_1 and τ_2, respectively, and A_1 and A_2 are a constants τ_1 and τ_2 are the decay times for the exponential components. The detailed fitting parameters are shown in Table 4.4. It is well known that the lifetime decreases with an increasing concentration of active ions due to the energy transfer between active ions, leading to concentration quenching. However, there is an increasing trend in the lifetime with an increasing Tb^{3+} concentration. Decay lifetimes for the $Sr_9La_{1-x}(PO_4)_7$: xTb^{3+} phosphors are estimated to be 2204, 2890, 3211, 3522, and 4062 μs, with x= 0.2, 0.4, 0.6, 0.8, and 1.0, respectively. Indeed, this difference is interesting and worth further investigation.

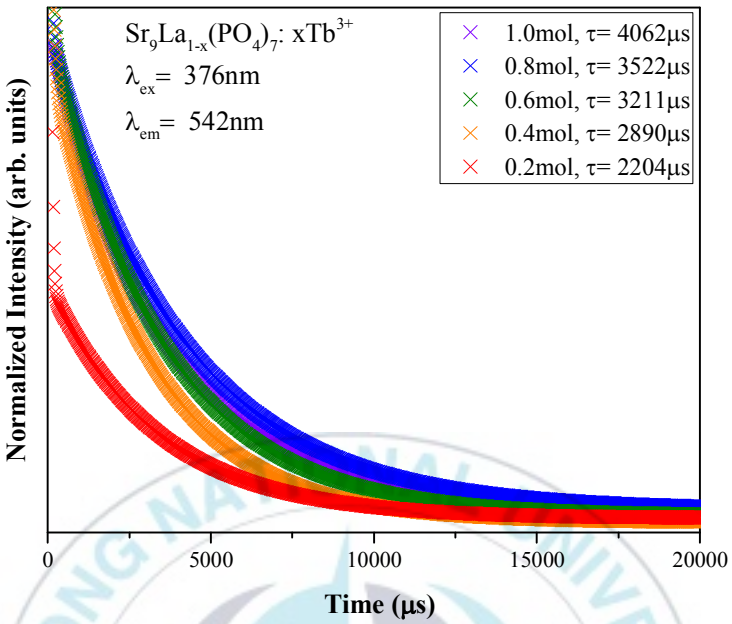

Fig. 4.13 Decay curves of $Sr_9La_{1-x}(PO_4)_7$: xTb^{3+} (x= 0.2, 0.4, 0.6, 0.8, 1).

Table 4.4 Fitting parameters of different decay curves for $Sr_9La(PO_4)_7$: xTb^{3+}.

Samples	A_1	τ_1(μs)	A_2	τ_2(μs)	τ(μs)
x= 0.2	9.316	32.22	0.180	3304	2204
x= 0.4	0.569	78.76	0.352	3009	2890
x= 0.6	0.919	63.04	0.377	3355	3211
x= 0.8	6.038	31.00	0.367	3970	3522
x= 1.0	0.103	1697	0.277	4401	4062

The energy transfer scheme of Tb^{3+} in the $Sr_9La(PO_4)_7$ host is shown in Fig. 4.14. Tb^{3+} ions absorb the energy from 376 nm irradiation and are excited from the ground state of $^7F_6$ to the excited state of ^5D_J. The Tb^{3+} concentration is high enough, and the emission from the $^5D_3$ level of Tb^{3+} is much weaker than the emission from the $^5D_4$ level due to cross-relaxation. Therefore, the blue emission is not seen, the excited Tb^{3+} relaxes to the low excited state $^5D_4$ through non-radiative transition, the radiative decay the ground state with a strong green emission.

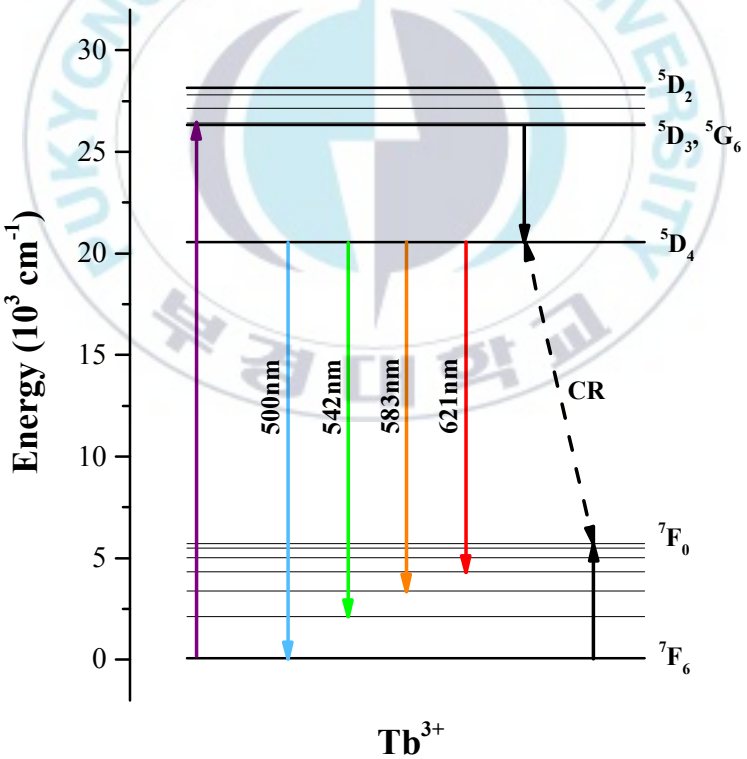

Fig. 4.14 Tb^{3+} energy level diagram.

. Conclusions

A series of $Sr_9La(PO_4)_7$: xSm^{3+} (x= 0.01, 0.03, 0.06, 0.09, 0.12) phosphors were successfully fabricated via a conventional solid-state reaction. The crystallographic analysis indicated that the doped $Sr_9La(PO_4)_7$: Sm^{3+} compounds crystallized in the rhombohedral crystal structure (space group: $R\bar{3}m$ (166)). The PL spectra of $Sr_9La(PO_4)_7$: xSm^{3+} samples were made up of four emission bands around 556, 595, 640, and 709 nm, corresponding to the $^4G_{5/2} \rightarrow {}^6H_J$ (J= 5/2, 7/2, 9/2, 11/2) transitions of Sm^{3+} ions, respectively. Among them, the $^7H_{5/2}$ was the most populated level. The optimal Sm^{3+} doping content turned out to be x= 0.03, and the critical transfer distance R_c of Sm^{3+} in $Sr_9La(PO_4)_7$ was determined to be 21.917 . The results pointed out that the $Sr_9La_{1-x}(PO_4)_7$: xSm^{3+} phosphors have a potential as orange-red phosphors for developing w-LEDs excited by n-UV radiation.

A series of novel $Sr_9La_{1-x}(PO_4)_7$: xTb^{3+} (x= 0.2, 0.4, 0.6, 0.8, 1) phosphors have been synthesized using the solid-state reaction method. From the XRD pattern analysis, it was confirmed that the crystal structure of the samples changed from rhombohedral (space group $R\bar{3}m$) to monoclinic (space group I2/a) with increase of the x value. The HRTEM image confirmed that some Tb^{3+} ion are substituted at the La^{3+} site in the space group $R\bar{3}m$ and the other are in the space group I2/a formed as $Sr_9Tb(PO_4)_7$. In other word, the phosphors except x=1 have mixed crystals with $R\bar{3}m$ and I2/a. The phosphors have a wide excitation band at the near-UV region due to the spin-allowed $4f^8 \rightarrow 4f^7 5d^1$ transitions of Tb^{3+} ions. Furthermore, the PL under the 376 nm excitation shows sharp high-intensity peaks

at approximately 542nm that have been ascribed to the transition between the excited state ($^7F_5$) and the ground state ($^5D_4$) of the Tb^{3+}. The PL intensity of $Sr_9La_{1-x}(PO_4)_7$: xTb^{3+} increased with an increasing Tb^{3+} concentration until a maximum intensity of about x= 1.0 was reached. It means that the concentration quenching of Tb^{3+} did not occur in the $Sr_9La(PO_4)_7$ host due to the $[PO4]^{3-}$ tetrahedron surrounds the luminescent center and acts as an obstacle between Tb^{3+} ions. The lifetimes monitored at 614 nm abnormally increased from 2204 to 4062 μs due to the crystal transformation with increasing of the concentration of Tb^{3+}. The results indicate that $Sr_9La(PO_4)_7$: Tb^{3+} could be an excellent candidate as a green-emitting phosphor.

References

[1] D. Kim, B.K. Moon, S.H. Park, J.H. Kim, J.H. Jeong, Full-color tuning in europium doped phosphosilicate phosphors via adjusting crystal field modulation or excitation wavelength, J. Alloys Compd. 770 (2019) 411–418.

[2] Y. Jin, Y. Fu, Y. Hu, L. Chen, H. Wu, G. Ju, M. He, T. Wang, A high color purity deep red emitting phosphor $SrGe_4O_9$: Mn^{4+} for warm white LEDs, Powder Technol. 292 (2016) 74–79.

[3] C.R. Ronda, T. Jüstel, H. Nikol, Rare earth phosphors: Fundamentals and applications, J. Alloys Compd. 275–277 (1998) 669–676.

[4] X. Zhang, L. Zhou, M. Gong, High-brightness Eu^{3+}-doped $Ca_3(PO_4)_2$ red phosphor for NUV light-emitting diodes application, Opt. Mater. (Amst). 35 (2013) 993–997.

[5] J. Zhao, C. Guo, J. Yu, R. Yu, Spectroscopy properties of Eu^{3+} doped $Ca_9R(VO_4)_7$ (R=Bi, La, Gd and Y) phosphors by sol-gel method, Opt. Laser Technol. 45 (2013) 62–68.

[6] H. Liu, Y. Zhang, L. Liao, Q. Guo, L. Mei, Synthesis, broad-band absorption and luminescence properties of blue-emitting phosphor $Sr_8La_2(PO_4)_6O_2$:Eu^{2+} for n-UV white-light-emitting diodes, Ceram. Int. 40 (2014) 13709–13713.

[7] M. Xia, X. Wu, Y. Zhong, H.T. Bert Hintzen, Z. Zhou, J. Wang, Photoluminescence properties and energy transfer in a novel $Sr_8ZnY(PO_4)_7$:Tb^{3+}, Eu^{3+} phosphor with high thermal stability and its

great potential for application in warm white light emitting diodes, J. Mater. Chem. C. 7 (2019) 2927–2935.

[8] J. Gou, J. Fan, M. Luo, S. Zuo, S. Ye, L. Ma, Y. Chen, M. Wang, X. Wang, B. Yu, $Sr_8ZnSc(PO_4)_7:Eu^{3+}$, Li^+ novel red-emitting phosphors: Synthesis and photoluminescence properties, Mater. Res. Bull. 86 (2017) 234–240.

[9] D. Xu, W. Zhou, Z. Zhang, X. Ma, Z. Xia, Luminescence property and energy transfer behavior of apatite-type $Ca_4La_6(SiO_4)_4(PO_4)_2O_2:Tb^{3+}$, Eu^{3+} phosphor, Mater. Res. Bull. 108 (2018) 101–105.

[10] Y. Xia, J. Chen, Y.G. Liu, M.S. Molokeev, M. Guan, Z. Huang, M. Fang, Crystal structure evolution and luminescence properties of color tunable solid solution phosphors $Ca_{2+x}La_{8-x}(SiO_4)_{6-x}(PO_4)_xO_2:Eu^{2+}$, Dalt. Trans. 45 (2016) 1007–1015.

[11] J. Cui, L. Wang, Q. Shi, Y. Tian, P. Huang, C. Cui, Color-tunable luminescence and energy transfer of Eu^{2+}/Mn^{2+} co-doped $Sr_9Lu(PO_4)_7$ phosphors for white LEDs, Polyhedron. 141 (2018) 284–288.

[12] P.A.M. Berdowski, G. Blasse, The critical concentration for quenching of the Eu^{3+} luminescence in some Gd^{3+} : Eu^{3+} systems, J. Solid State Chem. 63 (1986) 86–88.

[13] X. Kang, L. Wei, H. Wang, D. Ling, Energy Transfer from Ce^{3+} to Tb^{3+}/ Dy^{3+}/ Mn^{2+} in $Ca_9Ga(PO_4)_7$ Phosphors: Synthesis, Structure and Tunable Multicolor Luminescent Properties, ChemPhysChem. 20 (2019) 861–867.

[14] L. Li, X. Tang, Y. Zheng, Z. Wu, W. Chang, S. Jiang, G. Xiang, X. Zhou,

A novel dazzling Eu^{3+}-doped whitlockite-type phosphate red-emitting phosphor for white light-emitting diodes, J. Am. Ceram. Soc. 101 (2018) 4095–4107.

[15] L. Li, X. Tang, Z. Wu, Y. Zheng, S. Jiang, X. Tang, G. Xiang, X. Zhou, Simultaneously tuning emission color and realizing optical thermometry via efficient Tb^{3+}→Eu^{3+} energy transfer in whitlockite-type phosphate multifunctional phosphors, J. Alloys Compd. 780 (2019) 266–275.

[16] B. Ma, B. Liu, Luminescence properties and crystal structure of $Sr_3Sc(PO_4)_3$: Sm^{3+} as novel orange-red emitting phosphors, J. Lumin. 188 (2017) 54–59.

[17] L. Li, X. Tang, Z. Jiang, X. Zhou, S. Jiang, X. Luo, G. Xiang, K. Zhou, $NaBaLa_2(PO_4)_3$: A novel host lattice for Sm 3+ -doped phosphor materials emitting reddish-orange light, J. Alloys Compd. 701 (2017) 515–523.

[18] Y. Chen, Q. Guo, L. Liao, M. He, T. Zhou, L. Mei, M. Runowski, B. Ma, Preparation, crystal structure and luminescence properties of a novel single-phase red emitting phosphor $CaSr_2(PO_4)_2$:Sm^{3+}, Li^+, RSC Adv. 9 (2019) 4834–4842.

[19] C. Wang, J. Jiang, J. Wang, S. Xin, Y. Shi, G. Zhu, Novel high color purity phosphors $Sr_9Mg_{1.5}(PO_4)_7$: Sm^{3+}, R^+(R = Li, Na, K): Crystal structure, luminescence and thermal quenching property investigation, J. Lumin. 215 (2019) 116606.

[20] V. Singh, N. Singh, M.S. Pathak, P.K. Singh, V. Natarajan, Tb^{3+} doped

$Ca_2La_8(SiO_4)_6 O_2$ oxyapatite phosphors, Optik (Stuttg). 171 (2018) 356–362.

[21] K. Dorim, C. Byung Chun, P. Sung Heum, K. Jung Hwan, J. Kiwan, J. Jung Hyun, Full-color tuning by controlling the substitution of cations in europium doped $Sr_{8-x}La_{2+x}(PO_4)_{6-x}(SiO_4)_xO_2$ phosphors, Dye. Pigment. 160 (2019) 145–150.

[22] G.C. Kim, H.L. Park, T.W. Kim, Emission color tuning from blue to green through cross-relaxation in heavily Tb^{3+}-doped $YAlO_3$, Mater. Res. Bull. 36 (2001) 1603–1608.

[23] F. Yang, Z. Yang, Q. Yu, Y. Liu, X. Li, F. Lu, Sm3+-doped $Ba_3Bi(PO_4)_3$ orange reddish emitting phosphor, Spectrochim. Acta - Part A Mol. Biomol. Spectrosc. 105 (2013) 626–631.

[24] F.B. Xiong, H. Chen, H.F. Lin, X.G. Meng, E. Ma, W.Z. Zhu, Photoluminescence characteristics of Sm^{3+} -doped $LnBWO_6$ (Ln = La, Gd and Y) as new orange-red phosphors, J. Lumin. 209 (2019) 89–94.

[25] B.C. Jamalaiah, Optimization of photoluminescence of $GdAl_3(BO_3)_4:Sm^{3+}$ phosphors for solid state lighting devices, J. Mol. Struct. 1146 (2017) 546–553.

[26] X. Ma, L. Mei, H. Liu, L. Liao, Y. Liu, K. Nie, Z. Li, Structure and fluorescent properties of $Ba_3Sc(PO_4)_3:Sm^{3+}$ red-orange phosphor for n-UV w-LEDs, Chem. Phys. Lett. 653 (2016) 212–215.

[27] F. Yang, Y. Liu, X. Tian, G. Dong, Q. Yu, Luminescence properties of phosphate phosphor $Ba_3Y(PO_4)_3:Sm^{3+}$, J. Solid State Chem. 225 (2015)

19–23.

[28] J. Wu, M. Li, M. Wang, Z. Liu, H. Jia, Preparation and luminescence properties of $NaLa(WO_4)_2:Sm^{3+}$ orange-red phosphor, J. Lumin. 197 (2018) 219–227.

[29] L. Mei, H. Liu, L. Liao, Y. Zhang, R.V. Kumar, Structure and photoluminescence properties of red-emitting apatite-type phosphor $NaY_9(SiO_4)_6O_2:Sm^{3+}$ with excellent quantum efficiency and thermal stability for solid-state lighting, Sci. Rep. 7 (2017) 3–10.

[30] J. Sun, Y. Sun, Junhuizeng, H. Du, Luminescence properties and energy transfer investigations of $Sr_3Gd(PO_4)_3:Ce^{3+}$, Tb^{3+} phosphors, J. Phys. Chem. Solids. 74 (2013) 1007–1011.

[31] C. Zeng, Y. Hu, Z. Xia, H. Huang, A novel apatite-based warm white emitting phosphor $Ba_3GdK(PO_4)_3F:Tb^{3+}$, Eu^{3+} with efficient energy transfer for w-LEDs, RSC Adv. 5 (2015) 68099–68108.

[32] F. Zhang, W. YH, J. Zhang, L. BT, Y. Wen, Y. Tao, Photoluminescence Characteristics of $Ca_9Ln(PO4)_7:Tb^{3+}$ (Ln^{3+} = Y^{3+}, La^{3+}, Gd^{3+}) under VUV Excitation, Electrochem. Solid State Lett. 14 (2011) J16–J18.

[33] F. Xie, J. Li, Z. Dong, D. Wen, J. Shi, J. Yan, M. Wu, Energy transfer and luminescent properties of $Ca_8MgLu(PO_4)_7:Tb^{3+}/Eu^{3+}$ as a green-to-red color tunable phosphor under NUV excitation, RSC Adv. 5 (2015) 59830–59836.

[34] Q. Guo, C. Zhao, L. Liao, H. Liu, L. Mei, $KLaSr_3(PO_4)_3F$ (Re=$Tb^{3+}/Eu^{3+}/Eu^{2+}$): Promising Multi-Color Luminescence Phosphors

for n-UV/UV White LEDs, ChemistrySelect. 1 (2016) 2883–2888.

[35] X. Zhang, L. Zhou, J. Shi, M. Gong, Luminescence and energy transfer of a color tunable phosphor Tb^{3+}, Eu^{3+} co-doped $KCaY(PO_4)_2$, Mater. Lett. 137 (2014) 32–35.

[36] I. Carrasco, F. Piccinelli, M. Bettinelli, Optical Spectroscopy of $Ca_9Tb_{1-x}Eu_x(PO_4)_7$ (x = 0, 0.1, 1): Weak Donor Energy Migration in the Whitlockite Structure, J. Phys. Chem. C. 121 (2017) 16943–16950.

[37] R. Guo, S. Tang, B. Cheng, D. Tan, Y. Xiong, Synthesis and photoluminescence properties of a new green emitting phosphor $La_2SrB_{10}O_{19}:Tb^{3+}$, Opt. Mater. (Amst). 35 (2013) 1609–1611.

Acknowledgement

2 년의 석사과정을 마칠 수 있도록 부족한 저를 잘 이끌어주시고 이 논문을 완성하기까지 수많은 도움을 주신 분들께 감사의 말씀을 드리고 싶습니다.

먼저 타대학에서 진학한 저를 받아주시고 아낌없이 지원을 해주신 정중현 교수님께 깊은 감사의 뜻을 전합니다. 또한, 바쁘신 와중에도 소중한 시간을 내어 논문심사 해주시고 아낌없는 지도와 코멘트들로 큰 도움을 주셨던 김중환 교수님, 새로운 곳에 적응할 수 있도록 항상 관심 가져주시고 긍정적으로 가능성을 봐주시고 지원해주시는 박성흠 지도 교수님 덕분에 2 년의 석사과정 동안 많은 것을 배울 수 있었습니다. 그리고 타대학원에 진학한 저에게 길을 열어주신 장기완, 이호섭 교수님께도 감사의 말씀을 전하고 싶습니다.

아무것도 모르는 저에게 연구에 대한 방향과 방법을 처음부터 끝까지 알려줬던 도림 언니, 부족한 동생에게 항상 배려해주고 아낌없이 주는 언니 덕분에 석사과정을 무사히 마칠 수 있었습니다. 그리고 연구하면서 막히는 부분이 있을 때마다 많은 도움을 준 Xue Junpeng 에게도 감사의 마음을 전합니다. 그리고 형광소재은행 연구실의 최혜영 박사님, 서연우 박사님, 노현미 박사님 항상 챙겨주시고 웃는 얼굴로 맞이해 주셔서 감사합니다. 그리고 제가 적응할 수 있도록 신경 써주고 응원해줬던 이지훈 선배님, 신인수 선배님, 이달용 선배님, 양현석 선배님, Pesi, Zhang Yuanyuan, 단비 언니, 소영 언니 감사합니다. 그리고 석사과정을 무사히 마칠 수 있도록 기도해준 가족원 친구들에게도 감사의 인사를 드립니다.

언제나 저에게 힘이 되어주시고 든든한 기둥이 되어주신 사랑하는 아빠. 누구보다도 딸을 위해 기도해주고 응원해주신 사랑하는 엄마, 친구 같은 사랑스러운 은정이에게 감사의 인사를 전합니다. 마지막으로 이 모든 감사의 조건을 만들어주신 하나님께 감사드립니다.